

# Carbon uptake in Eurasian boreal forests dominates the high-latitude net ecosystem carbon budget

Jennifer D. Watts<sup>1</sup>  | Mary Farina<sup>1,2</sup> | John S. Kimball<sup>3</sup> | Luke D. Schiferl<sup>4,5</sup>  | Zhihua Liu<sup>3</sup> | Kyle A. Arndt<sup>1,6</sup> | Donatella Zona<sup>7</sup> | Ashley Ballantyne<sup>8</sup> | Eugénie S. Euskirchen<sup>9</sup> | Frans-Jan W. Parmentier<sup>10,11</sup> | Manuel Helbig<sup>12</sup> | Oliver Sonnentag<sup>13</sup> | Torben Tagesson<sup>11</sup>  | Janne Rinne<sup>11,14</sup> | Hiroki Ikawa<sup>15</sup> | Masahito Ueyama<sup>16</sup> | Hideki Kobayashi<sup>17</sup> | Torsten Sachs<sup>18</sup> | Daniel F. Nadeau<sup>19</sup> | John Kochendorfer<sup>20</sup> | Marcin Jackowicz-Korczynski<sup>11,21</sup> | Anna Virkkala<sup>1</sup> | Mika Aurela<sup>22</sup> | Roisin Commane<sup>4</sup> | Brendan Byrne<sup>23</sup> | Leah Birch<sup>1</sup> | Matthew S. Johnson<sup>24</sup> | Nima Madani<sup>23</sup> | Brendan Rogers<sup>1</sup> | Jinyang Du<sup>3</sup> | Arthur Endsley<sup>3</sup> | Kathleen Savage<sup>1</sup> | Ben Poulter<sup>25</sup> | Zhen Zhang<sup>26</sup> | Lori M. Bruhwiler<sup>27</sup> | Charles E. Miller<sup>23</sup> | Scott Goetz<sup>28</sup> | Walter C. Oechel<sup>7</sup>

<sup>1</sup>Woodwell Climate Research Center, Falmouth, Massachusetts, USA

<sup>2</sup>Department of Land Resources and Environmental Sciences, Montana State University, Bozeman, Montana, USA

<sup>3</sup>Numerical Terradynamic Simulation Group (NTSG), ISB 415, University of Montana, Missoula, Montana, USA

<sup>4</sup>Lamont-Doherty Earth Observatory, Columbia University, Palisades, New York, USA

<sup>5</sup>John A. Paulson School of Engineering and Applied Sciences, Harvard University, Cambridge, Massachusetts, USA

<sup>6</sup>Earth Systems Research Center, University of New Hampshire, Durham, New Hampshire, USA

<sup>7</sup>Global Change Research Group, Department of Biology, Physical Sciences 240, San Diego State University, San Diego, California, USA

<sup>8</sup>Global Climate and Ecology Laboratory, W.A. Franke College of Forestry and Conservation, University of Montana, Missoula, Montana, USA

<sup>9</sup>Institute of Arctic Biology, Fairbanks, Alaska, USA

<sup>10</sup>Department of Geosciences, Center for Biogeochemistry in the Anthropocene, University of Oslo, Oslo, Norway

<sup>11</sup>Department of Physical Geography and Ecosystem Science, Lund University, Lund, Sweden

<sup>12</sup>Department of Physics and Atmospheric Science, Dalhousie University, Halifax, Nova Scotia, Canada

<sup>13</sup>University of Montreal, Montreal, Quebec, Canada

<sup>14</sup>Natural Resources Institute Finland, Helsinki, Finland

<sup>15</sup>Hokkaido Agricultural Research Center, NARO, Sapporo, Japan

<sup>16</sup>Osaka Metropolitan University, Sakai, Japan

<sup>17</sup>JAMSTEC-Japan Agency for Marine-Earth Science and Technology, Yokohama, Japan

<sup>18</sup>GFZ German Research Centre for Geoscience, Potsdam, Germany

<sup>19</sup>Department of Civil and Water Engineering, Université Laval, Quebec City, Quebec, Canada

<sup>20</sup>NOAA Air Resources Laboratory, Atmospheric and Turbulent Diffusion Division, Oak Ridge, Tennessee, USA

<sup>21</sup>Department of Ecosystems, Aarhus University, Roskilde, Denmark

<sup>22</sup>Finnish Meteorological Institute, Helsinki, Finland

<sup>23</sup>Jet Propulsion Laboratory, California Institute of Technology, Pasadena, California, USA

<sup>24</sup>Biospheric Science Branch, NASA Ames Research Center, Moffett Field, California, USA

<sup>25</sup>NASA Goddard Space Flight Center, Greenbelt, Maryland, USA

<sup>26</sup>Department of Geographical Sciences, University of Maryland, College Park, Maryland, USA

Jennifer D. Watts and Mary Farina contributed equally to this publication.

Mary Farina shares first authorship for this article.

<sup>27</sup>NOAA Earth System Research Laboratory, Global Monitoring Division, Boulder, Colorado, USA<sup>28</sup>School of Informatics, Computing and Cyber Systems, Northern Arizona University, Flagstaff, Arizona, USA**Correspondence**

Jennifer D. Watts, Woodwell Climate Research Center, 149 Woods Hole Road, Falmouth, MA 02540, USA  
Email: [jwatts@woodwellclimate.org](mailto:jwatts@woodwellclimate.org)

**Funding information**

NASA, Grant/Award Number: 80NM0018D004, 80NSSC18K0770, 19-EARTH20-0105, NNX15AT74A and 80NSSC19M0113; NSF, Grant/Award Number: 1203583; Gordon and Betty Moore Foundation, Grant/Award Number: 8414

**Abstract**

Arctic-boreal landscapes are experiencing profound warming, along with changes in ecosystem moisture status and disturbance from fire. This region is of global importance in terms of carbon feedbacks to climate, yet the sign (sink or source) and magnitude of the Arctic-boreal carbon budget within recent years remains highly uncertain. Here, we provide new estimates of recent (2003–2015) vegetation gross primary productivity (GPP), ecosystem respiration ( $R_{\text{eco}}$ ), net ecosystem  $\text{CO}_2$  exchange (NEE;  $R_{\text{eco}} - \text{GPP}$ ), and terrestrial methane ( $\text{CH}_4$ ) emissions for the Arctic-boreal zone using a satellite data-driven process-model for northern ecosystems (TCFM-Arctic), calibrated and evaluated using measurements from >60 tower eddy covariance (EC) sites. We used TCFM-Arctic to obtain daily 1-km<sup>2</sup> flux estimates and annual carbon budgets for the pan-Arctic-boreal region. Across the domain, the model indicated an overall average NEE sink of  $-850 \text{ Tg CO}_2\text{-C year}^{-1}$ . Eurasian boreal zones, especially those in Siberia, contributed to a majority of the net sink. In contrast, the tundra biome was relatively carbon neutral (ranging from small sink to source). Regional  $\text{CH}_4$  emissions from tundra and boreal wetlands (not accounting for aquatic  $\text{CH}_4$ ) were estimated at  $35 \text{ Tg CH}_4\text{-C year}^{-1}$ . Accounting for additional emissions from open water aquatic bodies and from fire, using available estimates from the literature, reduced the total regional NEE sink by 21% and shifted many far northern tundra landscapes, and some boreal forests, to a net carbon source. This assessment, based on in situ observations and models, improves our understanding of the high-latitude carbon status and also indicates a continued need for integrated site-to-regional assessments to monitor the vulnerability of these ecosystems to climate change.

**KEY WORDS**

Arctic-boreal, carbon budget,  $\text{CH}_4$ ,  $\text{CO}_2$ , remote sensing, tundra, wetland

**1 | INTRODUCTION**

Northern tundra and boreal ecosystems store over half of the global soil organic carbon (SOC) pool (Hugelius et al., 2013; Schuur et al., 2015, 2022). Boreal ecosystems are estimated to account for 20% of the global forest carbon sink (Pan et al., 2011), with annual carbon uptake largely offsetting carbon dioxide ( $\text{CO}_2$ ) losses from respiration (Bradshaw & Warkentin, 2015). Some assessments of tundra indicate that arctic landscapes have been relatively near-neutral, varying between carbon sinks and sources (Belshe et al., 2013; Li et al., 2021; Virkkala et al., 2021). Other studies indicate trends toward net carbon source activity, especially in more recent years (Christensen et al., 2017; Commane et al., 2017; Natali et al., 2019; Schiferl et al., 2022; Watts et al., 2021). Additionally, boreal wetlands and many tundra environments are net emitters of methane ( $\text{CH}_4$ ; Kuhn et al., 2021; Strom & Christensen, 2007; Turetsky et al., 2014), which has a global warming potential 28–36 times higher

than  $\text{CO}_2$  over a 100-year period (Balcombe et al., 2018; Forster et al., 2021) and likely impacts the net ecosystem carbon budget (NECB;  $\text{CO}_2 + \text{CH}_4$ ).

Given the rapid warming occurring at high latitudes (Box et al., 2019; Chylek et al., 2022; Rantanen et al., 2022), the widespread thaw of permafrost (Biskaborn et al., 2019), lengthening of the annual non-frozen period (Kim et al., 2014), persistent thaw of deeper soil layers in winter (Commane et al., 2017; Zona et al., 2016), and increases in vegetation stress stemming from temperature extremes and drought (Pan et al., 2018; Peng et al., 2011; Phoenix & Bjerke, 2016; Wrona et al., 2016), there is concern that northern ecosystems are shifting closer toward a net source of carbon to the atmosphere (Abbott et al., 2016; Natali et al., 2019, 2021; Schuur et al., 2015; Zona et al., 2022). If just a fraction of the existing stored SOC is released (~1 trillion tonnes in the upper 1–3 m depth; Hugelius et al., 2013) through increased respiration and ecosystem disturbances, the magnitude could be comparable with

global deforestation rates (>200 billion tonnes C-CO<sub>2</sub> eq by 2100; Le Quéré et al., 2015).

Simultaneously, increases in vegetation cover at high latitudes, driven by shrubification and the drainage of water bodies, has led to more gross primary productivity (GPP) within some arctic regions (Bruhwiler et al., 2021; Mekonnen et al., 2021). However, decreases in vegetation CO<sub>2</sub> uptake, particularly in boreal forests following drought and disturbances, including fire, may substantially reduce these ecosystems' capacity to offset CO<sub>2</sub> losses from respiration (Bradshaw & Warkentin, 2015; Ribeiro-Kumara et al., 2020).

Various efforts have been taken to quantify high-latitude carbon budgets through field studies (e.g., Belshe et al., 2013; Euskirchen et al., 2017; Fox et al., 2008; Hashemi et al., 2021; Helbig et al., 2017; Ueyama et al., 2014), the statistical upscaling of in situ flux observations (Jung et al., 2020; Peltola et al., 2019; Virkkala et al., 2021), Earth system modeling (Birch et al., 2021; McGuire et al., 2012; Wang et al., 2019; White et al., 2001), and the combination of atmospheric observations and modeling (Ciais et al., 2010; Hartery et al., 2018; Schiferl et al., 2022; Sweeney et al., 2020; Tan et al., 2016; Welp et al., 2016). In situ field studies provide the most direct approach for understanding and monitoring ecosystem carbon status. Yet field sites represent only a very small fraction of the vast Arctic-boreal domain (Pallandt et al., 2022), and few sites offer continuous longer-term (>5 years) records of carbon flux (Schimel et al., 2015; Virkkala et al., 2022; Watts et al., 2021). Upscaling of in situ carbon fluxes through statistical modeling can be useful for obtaining "first look" estimates of regional carbon budgets. However, this non-mechanistic approach can be biased toward the underlying spatiotemporal representation of the input training data (limiting the ability of model extrapolation) and is often unable to represent dynamic shorter-term (i.e., daily to weekly) changes in carbon flux that might greatly influence seasonal and annual budget estimates.

Unlike statistical upscaling approaches, ecosystem (land-surface) models provide mathematical representations of underlying system processes including thermal and hydrologic states, and carbon cycle components (i.e., photosynthesis, carbon allocation and storage, autotrophic and heterotrophic respiration) and are often considered the "holy grail" of models. Even so, mechanistic models can have difficulty accurately reproducing complex ecosystem dynamics in arctic environments (Ballantyne et al., 2021; Chadburn et al., 2017; McGuire et al., 2012) and, as a result, these models have largely disagreed about the sink or source status of high-latitude carbon budgets (Euskirchen et al., 2022; Fisher et al., 2014; McGuire et al., 2012; Natali et al., 2019). Atmospheric inversion systems combine atmospheric transport models and observations of gas concentrations (e.g., point-based air samples from global flask networks and gas total column retrievals from satellites) to track carbon exchange and can be useful for indicating the overall carbon sink or source status across very large regions such as North American or Eurasian Arctic-boreal zones. However, these "top-down" models (often operating at resolutions >1° and, rarely, down to 5-km when well constrained by dense networks of regional observations, e.g., Ware et al., 2019) are unable to resolve more local patterns and ecosystem-level (<1-km)

contributions to carbon uptake or emission activity and are unable to project future carbon status (Ballantyne et al., 2021; Ciais et al., 2010; Commane et al., 2017; McGuire et al., 2012; Schimel et al., 2015). As a result, there is a continued need for the land surface-based, "bottom-up" accounting of carbon fluxes.

Eddy covariance (EC) flux tower systems (Baldocchi et al., 2001; Baldocchi & Koteen, 2012), positioned across the Arctic-boreal region (see Celis et al., 2020), provide high-frequency continuous measurements of land-atmosphere CO<sub>2</sub> and CH<sub>4</sub> exchange. At present, EC systems remain the most effective way to observe carbon, water, and energy fluxes at the landscape level (Baldocchi, 2020). Because EC towers only provide local observations, these data are often incorporated within statistical (Jung et al., 2020; Natali et al., 2019; Peltola et al., 2019; Ueyama et al., 2013; Virkkala et al., 2021), process-based (Birch et al., 2021; Jones et al., 2017; Watts, Kimball, Bartsch, et al., 2014; Watts, Kimball, Parmentier, et al., 2014), or data assimilation (Lopez-Blanco et al., 2019) model frameworks to obtain regional carbon estimates.

In this study, we used a satellite data-driven hybrid process-model for northern ecosystems, calibrated using observations from tower EC—that is, the Arctic Terrestrial Carbon Flux Model (TCFM-Arctic). Unlike highly complex mechanistic land-surface models, TCFM-Arctic was developed to simulate carbon cycle processes without the need for computationally intensive internal estimates of energy and moisture states. Instead TCFM-Arctic makes direct use of observations from remote sensing and reanalysis data to inform dynamic changes in ecosystem environmental conditions and their impact on CO<sub>2</sub> and CH<sub>4</sub> flux components. As a result, this deliberately simplified ecosystem model provides a powerful diagnostic tool for tracking contemporary carbon budgets across the high-latitude regions, obtaining improved estimate accuracy with reduced computational expense.

In this analysis, our objectives were to (1) obtain Arctic-boreal region estimates of terrestrial GPP, ecosystem respiration ( $R_{\text{eco}}$ ), net ecosystem CO<sub>2</sub> exchange (NEE), and CH<sub>4</sub> flux and (2) identify the status of flux budgets and regional patterns in ecosystem carbon sink and source activity, focused on the 2003–2015 period.

## 2 | MATERIALS AND METHODS

### 2.1 | Study domain

Our study domain encompassed terrestrial landscapes within the Arctic-boreal zone,  $\geq 50^{\circ}\text{N}$  (Figure 1). Most of this region remains frozen for more than half of the year (Kim et al., 2012, 2014). Approximately 84% of the domain is underlain by permafrost: 44% continuous; 14% discontinuous; and 26% sporadic or isolated permafrost (Brown et al., 2002). The colder, far northern, and higher-elevation regions are characterized by treeless tundra communities, including sedge wetlands, shrub, graminoids, moss, and more barren landscapes of herbs and lichen (CAVM, 2003). The warmer boreal region includes coniferous and deciduous forests of spruce, pine, aspen, birch, and larch (Table S1). Much of the boreal understory is moss dominated, with wetter areas falling

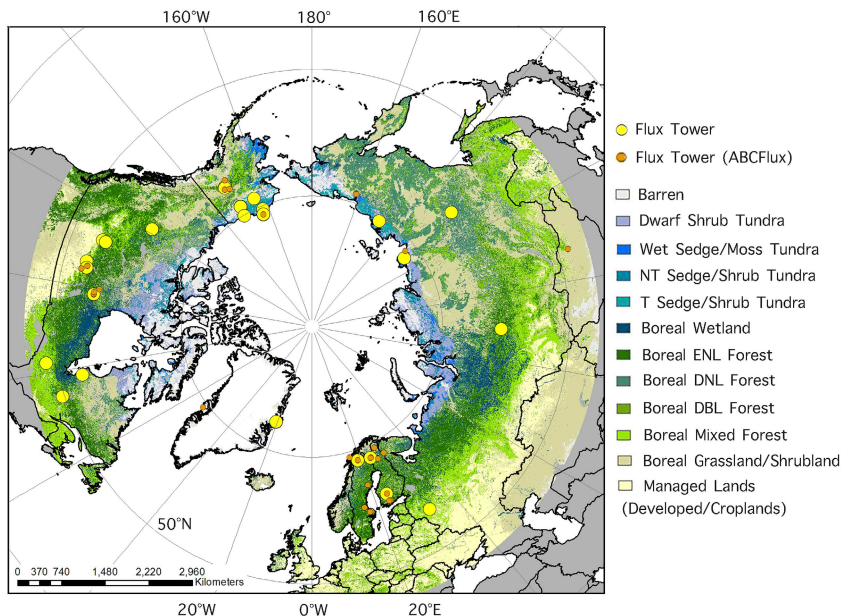


**FIGURE 1** Land cover for high-latitude regions (shown here extending down to 45°N) as derived from the merged ESA CCI-LC 2010 (Kirches et al., 2014) and Circumpolar Arctic Vegetation Map (CAVM; Walker et al., 2005). Yellow circles show EC flux tower sites from Table S1; orange circles denote EC sites from ABCFlux. Land cover classes include dwarf shrub tundra, non-tussock (NT) sedge/shrub tundra, tussock (T) sedge/shrub tundra, wet sedge/moss tundra, boreal wetland, boreal evergreen needleleaf forest (ENF), boreal deciduous needleleaf and broadleaf forests (DNF, DBL), boreal mixed forest, boreal grassland/shrubland, managed lands (developed, croplands), and sparse/barren lands.

into the category of peat-forming fens and bogs (Vitt, 2006). Our full study domain encompassed  $19.7 \times 10^6 \text{ km}^2$  ( $3.7 \times 10^6 \text{ km}^2$  in tundra regions,  $6 \times 10^6 \text{ km}^2$  in boreal forests,  $4.9 \times 10^6 \text{ km}^2$  in boreal wetlands, and  $5.1 \times 10^6 \text{ km}^2$  in boreal grassland/shrubland), extending into portions of the boreal zone that no longer have permafrost, and excluding open water, rock and ice, and barren lands.

For purposes of comparing estimated flux budgets with other regional analyses, we also considered the following sub-regions: (1) the far northern boreal and tundra RECCAP (REgional Carbon Cycle and Assessment Processes) domain (McGuire et al., 2012); (2) the NASA Arctic Boreal Vulnerability Experiment (ABOVE) domain that encompasses Alaska and northwestern Canada (Loboda et al., 2017); and (3) spatially distinct terrestrial biome regions (Dinerstein et al., 2017). A map of the sub-regions is provided in Figure S1.

## 2.2 | Flux tower CO<sub>2</sub> and CH<sub>4</sub> datasets

Flux data from EC towers were initially obtained for 35 tundra and boreal sites (Figure 1) across the Arctic-boreal region (Table S1). EC sites include ecosystems having permafrost classified as continuous (14 sites), discontinuous (6 sites) and sporadic/isolated (2 sites), and seasonal active layer thaw depths ranging from 20 cm (e.g., the more northern regions of Greenland, Russia, and North Slope Alaska) to >70 cm (e.g., Scandinavia, boreal Alaska, and Canada). The remaining 13 tower sites are located outside the permafrost zone but experience a strong seasonal freeze of surface and subsurface soils. The EC boreal sites best represent forests and wetlands; we were unable

to identify towers that represent mesic (non-forest, non-wetland) boreal shrubland/grasslands and, as a result, used an alternative model parameter assignment for this class (SI Section 1) that likely increased model estimate uncertainty.

The EC flux records were obtained through AmeriFlux, FluxNet, AsiaFlux, and individual tower principal investigators (PIs; Table S1). The EC records included half-hourly gap-filled NEE measurements partitioned into GPP and  $R_{\text{eco}}$  using methodology deemed appropriate by the tower PIs (e.g., Lasslop et al., 2010; Reichstein et al., 2012; Stoy et al., 2006). In addition to CO<sub>2</sub> flux, 15 of the sites also included half-hourly flux measurements of CH<sub>4</sub>. We used all of these tower observations for model calibration and verification, except for the NOAA Prudhoe tower (see SI Section 5.1.1). We also combined the GL-ZaF1 and GL-ZaF2 (wet fen tundra) fluxes because of their close spatial proximity. Thus, a total of 33 EC sites were used for model calibration and verification, representing over 56 site-years between 2003 and 2015. For independent model verification, we compared our model flux estimates against monthly-averaged EC observations provided through the Arctic-boreal CO<sub>2</sub> flux record (ABCFlux; Virkkala et al., 2022). ABCFlux provided us with 35 EC locations (11 tundra; 22 boreal forest; 2 boreal wetland; SI Section 5.1.2), after excluding EC sites (Table S1) that had been used for model calibration.

## 2.3 | The TCF model for Arctic-boreal ecosystems

The TCF model was developed as a precursor to the NASA Soil Moisture Active Passive (SMAP) mission Level 4 Carbon (L4\_C)

algorithms that are used to diagnose and reduce uncertainty and to provide remote sensing and EC data-informed carbon flux estimates, for global terrestrial carbon budgets (Jones et al., 2017; Kimball et al., 2009, 2016). The TCF model (Watts, Kimball, Parmentier, et al., 2014; and more recent versions, i.e., TCFM-Arctic) uses inputs from satellite optical remote sensing to infer changes in the fraction of photosynthetic active radiation absorbed by vegetation during carbon uptake. The model also incorporates satellite microwave retrievals that describe the daily surface frozen or unfrozen status (Kim et al., 2014). Meteorology inputs used in GPP and/or  $R_{\text{eco}}$  modules include daily incoming shortwave solar radiation ( $\text{W m}^{-2}$ ), atmospheric vapor pressure deficit (Pa), near-surface (~2 m) wind velocity ( $\text{m s}^{-1}$ ), 2 m air and ~10 cm depth soil temperature ( $^{\circ}\text{C}$ ;  $T_a$ ,  $T_s$ ), and root zone ( $\leq 1$  m depth) soil moisture ( $\text{RZ}_{\text{SM}}$ ;  $\text{m}^3 \text{m}^{-3}$ ) obtained from NASA Global Modeling and Assimilation Office (GMAO) 0.5° Modern-Era Retrospective analysis for Research and Applications (MERRA) Land fields (Reichle et al., 2011; Rienecker et al., 2011). The fraction of photosynthetic active radiation absorbed by vegetation through photosynthesis (FPAR) is obtained at a 1-km resolution from the Moderate Resolution Imaging Spectroradiometer (MODIS, MCD15A3H fields; Myneni et al., 2015). A more detailed description is provided in the SI Section 2.

The TCF model (Kimball et al., 2009) and SMAP L4\_C model parameter Look-Up-Table (LUT) logic (Jones et al., 2017; Kimball et al., 2016), based on generalized plant functional types (PFTs), was originally designed for global applications. The global LUT is based on Moderate Resolution Imaging Spectroradiometer (MODIS) mission Land Cover (MCD12Q1 Type 5) classes (e.g., Friedl et al., 2010) that do not fully characterize vegetation communities in Arctic-boreal ecosystems. For this study, we applied the TCFM-Arctic, a variant of the TCF model (adapted from Watts, Kimball, Parmentier, et al., 2014) designed to better represent northern high-latitude vegetation communities. The land cover products and classes used to guide TCFM-Arctic PFTs (Table S1), and calibration of GPP,  $R_{\text{eco}}$ , and  $\text{CH}_4$  module parameters according to the PFTs, are described in SI Sections 1 and 2. For TCFM-Arctic, we also improved representation of soil respiration processes during the cold season, by calibrating the model against a high-latitude winter respiration dataset (Natali et al., 2019; SI Section 1.2).

### 2.3.1 | TCFM-Arctic site-level assessments

Baseline carbon pools were initialized by continuously cycling ("spinning-up") the model for >1000 model years using a recent climatology from 1985 to 2002 (SI Section 1) to reach a dynamic steady-state between estimated net primary productivity (i.e.,  $\text{NPP} = \text{GPP} - \text{autotrophic respiration}$ ) and respiration from SOC stocks (following methods of Birch et al., 2021; Kimball et al., 2009; Watts, Kimball, Parmentier, et al., 2014). The resulting baseline SOC pools were incorporated as a starting point for the 2003 to 2015 forward model simulations. TCFM-Arctic uncertainty was assessed according to mean residual error (MRE; EC flux observations-model

flux estimates), root-mean-square error (RMSE), normalized RMSE (NRMSE;  $\text{RMSE}/|\bar{y}|$ ) and median/quartile differences. The resulting TCFM-Arctic EC tower site simulations were used to provide annual flux budgets for each site, which were summarized by tundra, boreal forest, and boreal wetland vegetation types for discussion purposes. We do not report site-level summary values for boreal grassland/shrublands because of lacking representation by the EC towers (SI Section 1.1). To gain an additional, independent, verification we evaluated our model estimates against 35 ABCFlux EC site records (Virkkala et al., 2022) that were not used in the TCFM-Arctic model calibration process.

### 2.3.2 | Regional flux budgets and model comparisons

The TCFM-Arctic simulations were extended to the Arctic-boreal domain, from 2003 to 2015, at a 1-km spatial resolution using land cover maps representing high-latitude vegetation communities (SI Section 2; Figure 1). Grid-cell flux estimates were aggregated to provide seasonal and annual carbon budgets over multiple regional domains. For the regional analyses, we excluded any grid cells where the land cover did not represent vegetated tundra or boreal communities (i.e., cropland, developed or barren regions). TCFM-Arctic does not account for carbon emissions from non-terrestrial aquatic environments; accordingly, we removed open-water areas when calculating terrestrial carbon budgets.

For the  $\text{CH}_4$  emission budgets, we primarily focused on grid cells classified as tundra or boreal wetland. As with any land cover type, the status and frequency of soil saturation often depends on landscape position. This sub-grid variability in wetness is extremely difficult to resolve using available (and typically coarser-scale) soil moisture products. To address this, we further constrained  $\text{CH}_4$  emission budgets using a topographic wetness index (TWI)-based masking approach (SI Section 3). For the boreal region, we compared our  $\text{CH}_4$  estimates with and without including a boreal peatland class, in addition to the grid cells classified as boreal wetland. As our model does not yet estimate  $\text{CH}_4$  uptake because of lack of detailed regional uptake observations to inform process modeling, we provide an estimate of uptake for upland areas using recent synthesis estimates of this flux for high latitudes (SI Section 6).

We compared the resulting TCFM-Arctic budgets with regional flux estimates (SI Section 8) from an Arctic-boreal version of the Community Land Model Version 5 (CLM 5; Birch et al., 2021); satellite-informed SMAP L4\_C and MODIS (MOD17A2H)  $\text{CO}_2$  flux products (Kimball et al., 2012; Running et al., 2004); statistically upscaled  $\text{CO}_2$  estimates from Virkkala et al. (2021) and FluxCom (Jung et al., 2020); statistically upscaled  $\text{CH}_4$  estimates from Peltola et al. (2019), and results from atmospheric inversions—Atmospherically-enhanced Inversion (ACI) models (Liu et al., 2020, 2022) and the v10 Orbiting Carbon Observatory-2 inversion modeling intercomparison project (v10 OCO-2 MIP; Byrne, Baker, et al., 2022; Byrne, Liu, et al., 2022) experiments. Additionally, we evaluated our terrestrial  $\text{CH}_4$  emission

estimates against assimilation records from CarbonTracker-CH<sub>4</sub> (Bruhwiler et al., 2014).

We used FluxCom ensemble carbon flux products based on MODIS remote sensing (RS; 0.5° spatial resolution) and based on MODIS plus meteorological data (RS+METEO; 0.5° spatial resolution) (Jung et al., 2020). Statistically upscaled CH<sub>4</sub> estimates from Peltola et al. (2019) were provided using three different wetland maps, including the static global wetland map PEATMAP (Xu et al., 2018), the dynamic wetland map based on DYPTOP (Dynamical Peatland Model Based on TOPMODEL; Stocker et al., 2014), and the Global Lakes and Wetlands Database (GLWD; Lehner & Döll, 2004).

To identify patterns of multi-year (2003–2015) change in the regional Arctic-boreal flux records we applied the Yue Pilon (2002) monotonic approach which pre-whitens the data record to remove the effects of autocorrelation prior to applying a Mann-Kendall test for trend significance and calculating Sen's slope (Watts, Kimball, Bartsch, et al., 2014). This was performed using the R computing language (R Core Team, 2019) 'Zyp' package (Bronaugh & Werner, 2019). We report trends with caution, given the relatively short (13-year) study record. Lastly, to examine the impact of aquatic CH<sub>4</sub> and terrestrial fire carbon emissions on the regional budgets, we included information from the Johnson et al. (2021, 2022) open water CH<sub>4</sub> emissions products, and the Global Fire Emissions Database version 5 (GFEDv5; van Wees et al., 2022) for a more complete assessment of NECB.

## 3 | RESULTS

### 3.1 | Flux characteristics at eddy covariance sites

#### 3.1.1 | Flux patterns and environmental constraints

A summary of the flux characteristics for the EC sites is found in the SI Section 5. The EC observations showed the annual start of boreal GPP beginning late March into mid-April (e.g., Scotty Creek and Lompolojäkkä boreal towers; Figure S2) and persisting until early November. The growing season in tundra was much shorter (e.g., Utqiāġvik and Ivotuk towers; Figure S2), beginning in late June and lasting into September or early October.  $R_{\text{eco}}$  followed a similar pattern, but CO<sub>2</sub> emissions were also substantial in spring (as the soils thawed) and autumn (as the soils froze) and often persisted into winter at more southern sites. Emissions of CH<sub>4</sub> in tundra and boreal wetlands peaked in later (solar) summer (June–August) when soils were warmest and more labile carbon was available from recent photosynthates or thawed soil organics. As with  $R_{\text{eco}}$ , CH<sub>4</sub> emissions were observed during the non-growing season.

Figure 2 shows the observed, often non-linear relationships between primary environmental drivers and EC carbon fluxes. This non-linearity is also reflected in the TCFM-Arctic modules. GPP,  $R_{\text{eco}}$  and NEE increased exponentially with temperature. Emissions of CO<sub>2</sub> and CH<sub>4</sub> were observed at temperatures well below freezing, and the CH<sub>4</sub> flux rose substantially when soil temperatures

exceeded 0°C. The relationships between soil moisture and CO<sub>2</sub> flux components (i.e., GPP and  $R_{\text{eco}}$ ) were more variable relative to temperature and fluxes were generally higher under mesic soil conditions, whereas CH<sub>4</sub> emissions increased with soil wetness.

#### 3.1.2 | Comparison of model simulations with eddy covariance fluxes

The daily 1-km<sup>2</sup> TCFM-Arctic simulations, driven using relatively coarse reanalysis and satellite inputs, provided reasonably accurate estimates (Figure S3) of daily fluxes relative to the EC observations (Table S1), with the RMSE for NEE averaging 0.8 g CO<sub>2</sub>-C m<sup>-2</sup> day<sup>-1</sup> (Table S5). The average RMSEs for GPP and  $R_{\text{eco}}$  were 1.2 and 0.9 g CO<sub>2</sub>-C m<sup>-2</sup> day<sup>-1</sup>, respectively. Accounting for large differences in flux magnitudes between boreal and tundra showed a slightly larger GPP NRMSE (i.e., standardized RMSE) in tundra (0.8) relative to boreal (0.6), primarily because TCFM-Arctic indicated an earlier (by ~1 week) annual start of growing season (where GPP > 0) in tundra relative to the EC records.  $R_{\text{eco}}$  NRMSE values were similar between boreal and tundra (~0.8). RMSE for CH<sub>4</sub> was 23 mg CH<sub>4</sub>-C m<sup>-2</sup> day<sup>-1</sup>, with higher uncertainty observed in boreal wetlands relative to tundra (NRMSE 1.4 vs. 1). Evaluating TCFM-Arctic against independent CO<sub>2</sub> observations from ABCFlux (Table S5) indicated NEE RMSEs (g CO<sub>2</sub>-C m<sup>-2</sup> day<sup>-1</sup>) of: 0.7 for tundra; 0.8 for boreal forests; and 0.6 for boreal wetlands. Associated NRMSEs for the ABCFlux comparisons were 2.5 (tundra), 3.8 (boreal forests), and 5.4 (boreal wetlands).

TCFM-Arctic was unable to account for episodic CO<sub>2</sub> and CH<sub>4</sub> emissions that occurred during spring thaw and autumn freeze events, particularly in tundra (e.g., see Figure S2, Ivotuk). This contributed to lower TCFM-Arctic estimates of total annual  $R_{\text{eco}}$  and NEE relative to annual budgets based on EC observations. For example,  $R_{\text{eco}}$  for tundra sites in autumn (September, October) and spring (April, May) was, on average, 82% and 73% less than the EC flux-derived estimates. The model underestimated CH<sub>4</sub> emissions from boreal wetlands in summer (June–August) and autumn by, on average, 28% and 49%, most likely due to the difficulty of estimating ebullitive flux during the non-frozen period and diffusive flux during soil freeze. The model also underestimated tundra CH<sub>4</sub> emissions by 40% during the autumn freeze.

### 3.2 | TCFM-Arctic flux budgets

#### 3.2.1 | Annual carbon budgets at eddy covariance tower sites

Based on the (Table S1) EC records, the annual across-site NEE budget averages ( $\pm$  across-site stdev) were  $-46 \pm 245$  g CO<sub>2</sub>-C year<sup>-1</sup> (boreal forests),  $-86 \pm 133$  g CO<sub>2</sub>-C year<sup>-1</sup> (boreal wetlands), and  $75 \pm 104$  g CO<sub>2</sub>-C year<sup>-1</sup> (tundra). The NEE budgets (g CO<sub>2</sub>-C year<sup>-1</sup>) from TCFM-Arctic were  $-47 \pm 112$  (boreal forests),  $-48 \pm 72$  (boreal wetlands), and  $36 \pm 57$  (tundra). Because of the 1-km<sup>2</sup> TCFM-Arctic

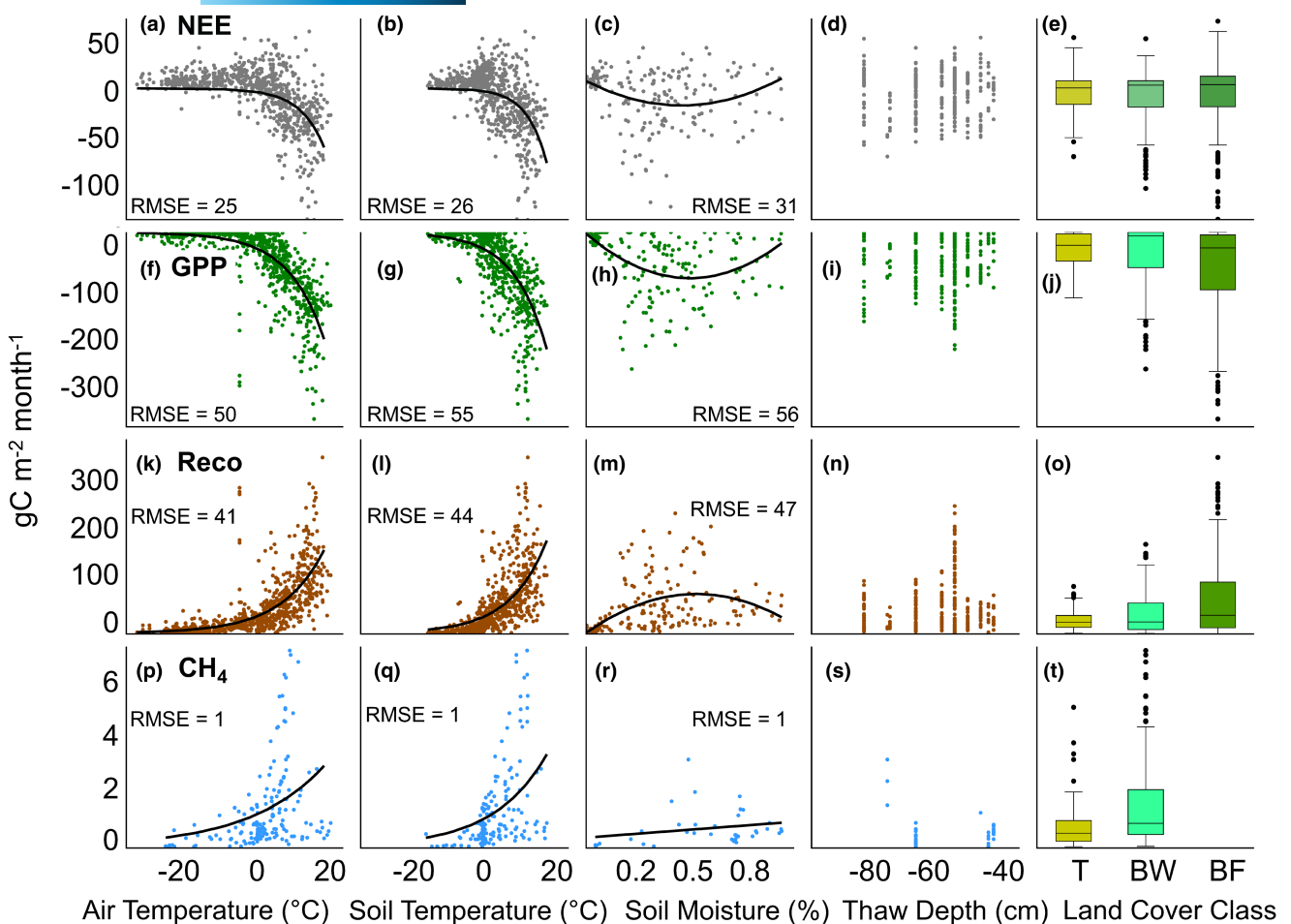


**FIGURE 2** Relationships between monthly average carbon fluxes obtained from eddy covariance (EC) tower records; in situ temperature, soil moisture, and thaw depth (for permafrost environments) from EC site measurements for different land cover classes (tundra (T), boreal wetlands (BW), and boreal forest (BF)). The carbon flux components are NEE, GPP (provided as negative values here to indicate carbon uptake),  $R_{\text{eco}}$ , and CH<sub>4</sub> in units of gC m<sup>-2</sup> month<sup>-1</sup>. Shown here are the relationships of NEE versus (a) air temperature, (b) soil temperature at 5 cm depth, (c) soil moisture, (d) thaw depth, (e) land cover class; GPP versus (f) air temperature, (g) soil temperature, (h) soil moisture, (i) thaw depth, (j) land cover class;  $R_{\text{eco}}$  versus (k) air temperature, (l) soil temperature, (m) soil moisture, (n) thaw depth, (o) land cover class; CH<sub>4</sub> versus (p) air temperature, (q) soil temperature, (r) soil moisture, (s) thaw depth, (t) land cover class. Corresponding equations for the fitted lines are found in Table S3. We did not examine relationships between carbon fluxes and in situ observations of deeper soil temperatures and depth of water table because these were not available across sites. Negative values for thaw indicate depth below surface.

footprint, the model estimates are likely to encompass trees adjacent to wetlands, which results in larger CO<sub>2</sub> uptake relative to EC tower estimates. The EC-estimated (TCFM-Arctic) CH<sub>4</sub> emissions were  $9.7 \pm 6$  ( $6.9 \pm 4$ ) gCH<sub>4</sub>-Cyear<sup>-1</sup> (boreal wetlands) and  $5.7 \pm 5$  ( $3.2 \pm 2.5$ ) gCH<sub>4</sub>-Cyear<sup>-1</sup> (tundra). See Table S6 for corresponding seasonal budgets.

According to TCFM-Arctic, the largest forest NEE sinks were at a large site in Siberia (RU-Skp;  $-86$  gCO<sub>2</sub>-Cm<sup>-2</sup> year<sup>-1</sup>), followed by a mature aspen forest in Canada (CA-Oas;  $-83$  gCO<sub>2</sub>-Cm<sup>-2</sup> year<sup>-1</sup>). In comparison, an NEE source occurred in southern old growth spruce (RU-Fyo;  $7$  gCO<sub>2</sub>-Cm<sup>-2</sup> year<sup>-1</sup>) stands. The boreal wetland sites were net sinks, with the largest NEE occurring in a southern peatland (CA-WP1;  $-97$  gCO<sub>2</sub>-Cm<sup>-2</sup> year<sup>-1</sup>) and the lowest in a northern bog (CA-SCB;  $-34$  gCO<sub>2</sub>-Cm<sup>-2</sup> year<sup>-1</sup>). NEE activity at the tundra sites varied from sink to source. NEE sink was highest at the US-ICT and US-Ivo tussock tundra sites in Alaska ( $-13$  and

$-11$  gCO<sub>2</sub>-Cm<sup>-2</sup> year<sup>-1</sup>) whereas the largest source occurred in the far northern Siberian tundra (RU-Sam;  $7$  gCO<sub>2</sub>-Cm<sup>-2</sup> year<sup>-1</sup>). Two warmer boreal fens in Finland (FI-SII and FI-Lom) had the highest CH<sub>4</sub> emissions ( $\sim 14$  and  $13$  gCH<sub>4</sub>-Cm<sup>-2</sup> year<sup>-1</sup>); the lowest emissions ( $\sim 0.5$ – $0.6$  gCH<sub>4</sub>-Cm<sup>-2</sup> year<sup>-1</sup>) were in far-northern tundra (RU-Sam and US-Beo).

### 3.2.2 | Annual carbon budgets for Arctic-boreal domain

Our regional model estimates (Table 1; Figures 3–5) indicated an NEE budget of  $-601 \pm 1138$  TgCO<sub>2</sub>-Cyear<sup>-1</sup> when including boreal forests, boreal wetlands, and tundra. This uncertainty is based on RMSE using independent monthly-average EC tower observations from ABCFlux (SI Section 7). The associated RMSE-based uncertainty

using the daily-average **Table 1** EC fluxes was 744 Tg CO<sub>2</sub>-C year<sup>-1</sup>. When we included the boreal shrubland/grassland class, for which we have lower confidence due to absent coverage by EC towers, the Arctic-boreal sink was -850 Tg CO<sub>2</sub>-C year<sup>-1</sup>. The tundra region had a small average CO<sub>2</sub> sink status (**Figure 4**; -16 Tg CO<sub>2</sub>-C year<sup>-1</sup>; -4 g CO<sub>2</sub>-C m<sup>-2</sup> year<sup>-1</sup>) and was carbon neutral when considering the range of uncertainty ( $\pm 84$ –270 Tg CO<sub>2</sub>-C year<sup>-1</sup>; based on RMSEs from **Table S1** and ABCFlux sites). Boreal regions were CO<sub>2</sub> sinks of -311 Tg CO<sub>2</sub>-C year<sup>-1</sup> (-52 g CO<sub>2</sub>-C m<sup>-2</sup> year<sup>-1</sup>) in forests and -274 Tg CO<sub>2</sub>-C year<sup>-1</sup> (-56 g CO<sub>2</sub>-C m<sup>-2</sup> year<sup>-1</sup>) in wetlands, with uncertainties of  $\pm 405$ –546 and  $\pm 256$ –322 Tg CO<sub>2</sub>-C year<sup>-1</sup>.

Across the full domain, winter (November–March) and autumn (September, October) seasons were net CO<sub>2</sub> sources (NEE of 875 and 69 Tg CO<sub>2</sub>-C year<sup>-1</sup> respectively), while spring (April, May) and summer (June–August) seasons were net CO<sub>2</sub> sinks (NEE of -223 and -1572 Tg CO<sub>2</sub>-C year<sup>-1</sup>). Eurasia contributed to most (74%) of the annual Arctic-boreal NEE sink (**Table S9a**), primarily within the eastern boreal zone, whereas North America only contributed to 26% of the total NEE sink. At the ecosystem level (**SI Section 9**; **Table S10**), the East Siberian Taiga, the West Siberian Taiga, and the Scandinavian and Russian Taiga had the largest contributions (i.e., 27%, 8%, and 7%) to the total Arctic-boreal NEE sink. The East Canadian Shield Taiga Ecoregion had the largest NEE sink in North America. On a per-m<sup>2</sup> basis, the Chinese Da Hinggan-Dzhagdy Mountains bordering Russia, and the Kamchatka-Kurile Meadows in the Russian Far East, had the highest NEE uptake ( $\sim 73$  g CO<sub>2</sub>-C m<sup>-2</sup> year<sup>-1</sup>), and were characterized by moist, mild summers, and an absence of permafrost.

The Arctic-boreal CH<sub>4</sub> budget was estimated at 35 Tg CH<sub>4</sub>-C year<sup>-1</sup> (see **SI Section 6** for a discussion of CH<sub>4</sub> budgets when including peatlands). A majority of emissions ( $\geq 82\%$ , **Table S8**)

were from the boreal zone. Eurasia (particularly the vast wetlands in Russia) contributed 65% of total CH<sub>4</sub> emissions (**Figure 4**). Our estimate of CH<sub>4</sub> uptake (-4 Tg CH<sub>4</sub>-C year<sup>-1</sup>; **SI Section 6**) was relatively minimal.

The TCFM-Arctic GPP budget for the full domain remained relatively stable over the 2003–2015 period, with short-term increases observed in 2007, 2009, 2011–2012, and 2014 (**Figure 5**). A significant GPP decline (**SI Section 9.5**) was detected for North America tundra, primarily driven by lower summer GPP, and for North America forests in spring and summer. A small but significant increase in annual GPP was detected for boreal wetlands in Eurasia. Eurasia tundra in spring and North America tundra in autumn had a small increase in annual NEE sink. A significant increase in the boreal forest annual NEE sink was detected for Eurasia, driven by strong sink activity in spring. In contrast, North America boreal forests had reduced NEE sink strength driven by lower summer NEE. For wetland CH<sub>4</sub>, there was a small but significant increase in emissions for Eurasia tundra, particularly in summer and autumn. A decrease in annual CH<sub>4</sub> emissions was detected for tundra in North America. In boreal wetlands, an increase in CH<sub>4</sub> emissions was identified in Eurasia during spring, which was countered by lower emissions in autumn.

### 3.2.3 | Comparison of TCFM-Arctic net ecosystem CO<sub>2</sub> exchange with other modeled budgets

The TCFM-Arctic results compared with estimates from other bottom-up models and atmospheric inversions (**Tables S9B–I**) showed large variability in the sign and magnitude of NEE activity for the tundra region (see **Figures S7–S9** for NEE, GPP, and

**TABLE 1** Annual total carbon budgets (Tg C year<sup>-1</sup>) across the Arctic-boreal domain considering TCFM-Arctic informed NEE and NECB in terms of: NEE + terrestrial (non-aquatic wetland) CH<sub>4</sub> emissions; NEE + terrestrial CH<sub>4</sub> emissions + aquatic open water CH<sub>4</sub> emissions (Johnson et al., 2021, 2022), and carbon emissions from wildfires (GFEDv5; van Wees et al., 2022)

Region	NEE	NEE + CH <sub>4</sub>	NEE + CH <sub>4</sub> + open water CH <sub>4</sub>	NEE + CH <sub>4</sub> + open water CH <sub>4</sub> + fire
All tundra and boreal (EU + NA)	-850	-815	-810	-640
Tundra (EU + NA)	-16	-9.4	-8.2	-6.2
Tundra (EU)	-10.5	-6.7	-6.3	-5.2
Tundra (NA)	-5.1	-2.7	-1.9	-1
Boreal forest (EU + NA)	-311	-311	-310	-216
Boreal forest (EU)	-248	-248	-247	-199
Boreal forest (NA)	-63	-63	-62	-17
Boreal wetland (EU + NA)	-274	-246	-244	-204
Boreal wetland (EU)	-190	-171	-171	-149
Boreal wetland (NA)	-84	-75	-74	-56
Boreal grasslands/shrubland (EU + NA)	-249	-249	-248	-213
Grasslands/shrublands (EU)	-181	-181	-181	-158
Grasslands/shrublands (NA)	-68	-68	-67	-55

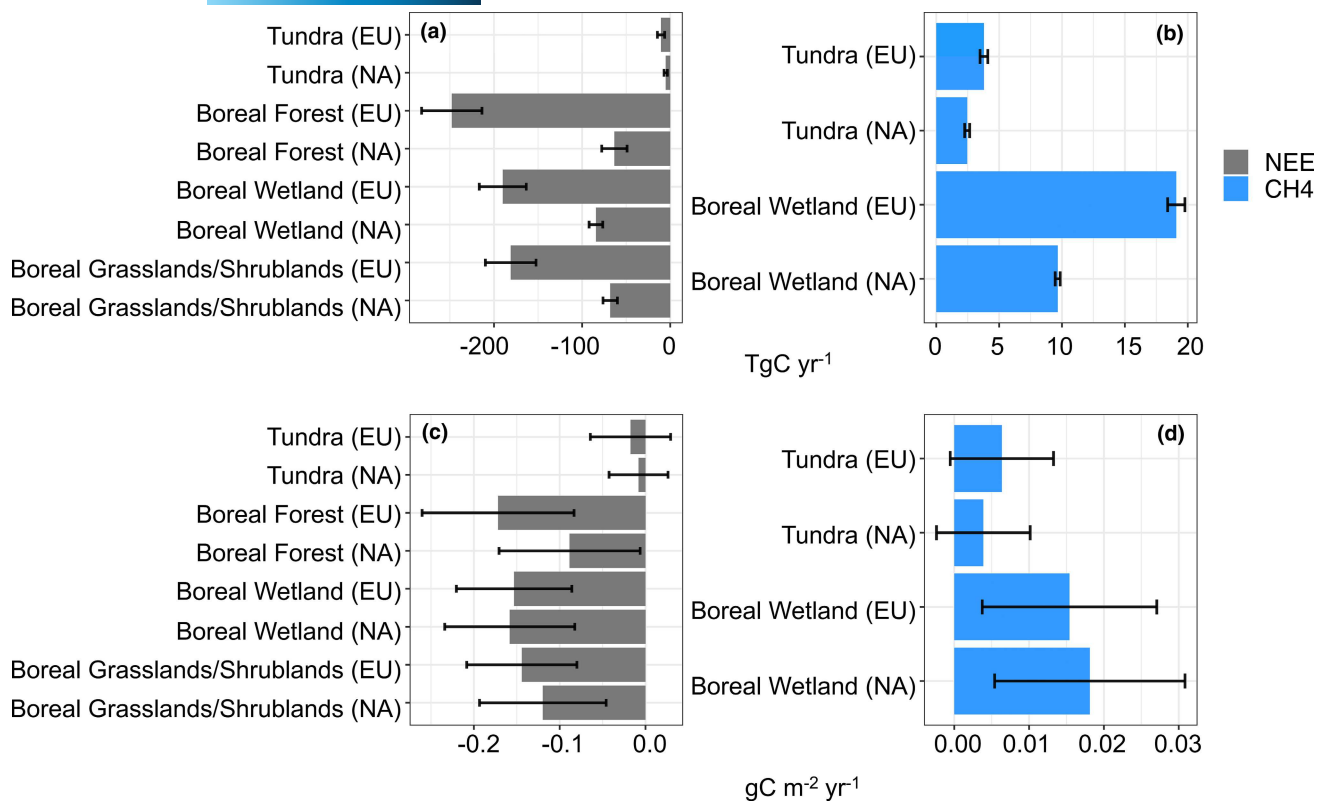


**FIGURE 3** Average TCFM-Arctic annual budgets ( $\text{Tg C year}^{-1}$ ) by region for (a) net ecosystem  $\text{CO}_2$  exchange (NEE) and (b)  $\text{CH}_4$  emissions. In addition, annual budgets normalized by area ( $\text{g C m}^{-2} \text{ day}^{-1}$ ) are provided for NEE (c) and  $\text{CH}_4$  (d). Regions are defined as tundra, boreal forests, boreal wetlands, or boreal shrublands/grasslands within Eurasia (EU) or North America (NA).

$R_{\text{eco}}$  budgets). SMAP L4\_C and CLM 5.0 indicated a small NEE source (8 and  $21 \text{ Tg CO}_2 \text{-C year}^{-1}$ ), relative to a much larger source ( $245 \text{ Tg CO}_2 \text{-C year}^{-1}$ ) estimated by FluxCom RS. Whereas TCFM-Arctic, the ACI ensemble (Liu et al., 2020), the OCO-2 MIP experiments (Byrne, Baker, et al., 2022; Byrne, Liu, et al., 2022), FluxCom RS+METEO and Virkkala et al. (2021) showed a small to moderate NEE sink ( $-16$ ,  $-21$ ,  $-49$  to  $-32$ ,  $-80$ ,  $-97 \text{ Tg CO}_2 \text{-C year}^{-1}$ , respectively).

Variability in NEE estimates was also observed within the boreal zone. For Eurasia forests, five models (FluxCom RS, FluxCom RS+METEO, TCFM-Arctic, OCO-2 MIP, Virkkala et al., 2021, ACI ensemble) indicated a relatively strong NEE sink ( $-398$ ,  $-303$ ,  $-248$ ,  $-377$  to  $-196$ ,  $-154$ ,  $-122 \text{ Tg CO}_2 \text{-C year}^{-1}$ ) compared with a more moderate sink reported by CLM 5.0 ( $-99 \text{ Tg CO}_2 \text{-C year}^{-1}$ ). Whereas, SMAP L4\_C showed a source of  $51 \text{ Tg CO}_2 \text{-C year}^{-1}$ . Across the North American boreal forests, FluxCom RS, OCO-2 MIP, FluxCom RS+METEO, ACI ensemble, Virkkala et al. (2021), TCFM-Arctic, and CLM 5.0 models reported a strong to moderate NEE sink ( $-243$ ,  $-211$  to  $-144$ ,  $-153$ ,  $-75$ ,  $-69$ ,  $-63$ ,  $-42 \text{ Tg CO}_2 \text{-C year}^{-1}$ ), while SMAP L4\_C showed a much smaller NEE sink ( $-3.6 \text{ Tg CO}_2 \text{-C year}^{-1}$ ).

Most of the models (TCFM-Arctic, OCO-2 MIP, FluxCom RS+METEO, Virkkala et al., 2021, ACI ensemble, and CLM 5.0) indicated various levels of NEE sink strength in boreal wetland complexes ( $-274$ ,  $-253$  to  $-97$ ,  $-161$ ,  $-122$ ,  $-103$ ,  $-44 \text{ Tg CO}_2 \text{-C year}^{-1}$ ,

except for two models (SMAP L4\_C and FluxCom RS) indicating NEE sources ( $45$ ,  $77 \text{ Tg CO}_2 \text{-C year}^{-1}$ ). The Virkkala et al. (2021), TCFM-Arctic, OCO-2 MIP, FluxCom RS+METEO, ACI ensemble, and CLM 5.0 models estimated a NEE sink for boreal grassland/shrublands ( $-205$ ,  $-249$ ,  $-254$  to  $-93$ ,  $-142$ ,  $-96$ ,  $-39 \text{ Tg CO}_2 \text{-C year}^{-1}$ ); whereas, SMAP L4\_C and FluxCom RS estimated a NEE source ( $46$ ,  $85 \text{ Tg CO}_2 \text{-C year}^{-1}$ ).

Results from the  $\text{CH}_4$  comparisons (for terrestrial tundra and boreal wetlands, excluding open water aquatic areas) indicated annual emissions of  $4$ – $6 \text{ Tg CH}_4 \text{-C year}^{-1}$  from Eurasian tundra according to TCFM-Arctic and CLM 5.0, compared with Peltola et al. (2019) machine-learning model estimates which were  $\sim 0.45 \text{ Tg CH}_4 \text{-C year}^{-1}$  (Figure S10). In North American tundra, the emission estimates ranged from around  $2 \text{ Tg CH}_4 \text{-C year}^{-1}$  (TCFM-Arctic, CLM 5.0) down to  $1$ – $0.05 \text{ Tg CH}_4 \text{-C year}^{-1}$  for the Peltola et al. (2019) results. The TCFM-Arctic estimate for Eurasian boreal wetlands was  $19 \text{ Tg CH}_4 \text{-C year}^{-1}$ , which is higher than the other bottom-up models (around  $3$ – $8 \text{ Tg CH}_4 \text{-C year}^{-1}$ ). For boreal wetlands of North America, the TCFM-Arctic estimates were also higher ( $9.7 \text{ Tg CH}_4 \text{-C year}^{-1}$ ) compared with the other bottom-up models ( $2.6$ – $5 \text{ Tg CH}_4 \text{-C year}^{-1}$ ). For the entire Arctic-boreal region, our results were very similar to CarbonTracker- $\text{CH}_4$  (averaging  $35.5 \text{ Tg CH}_4 \text{-C year}^{-1}$ ), though the TCFM-Arctic results were 34% higher than CarbonTracker- $\text{CH}_4$  over the North America domain and 19% lower in Arctic-boreal Eurasia.

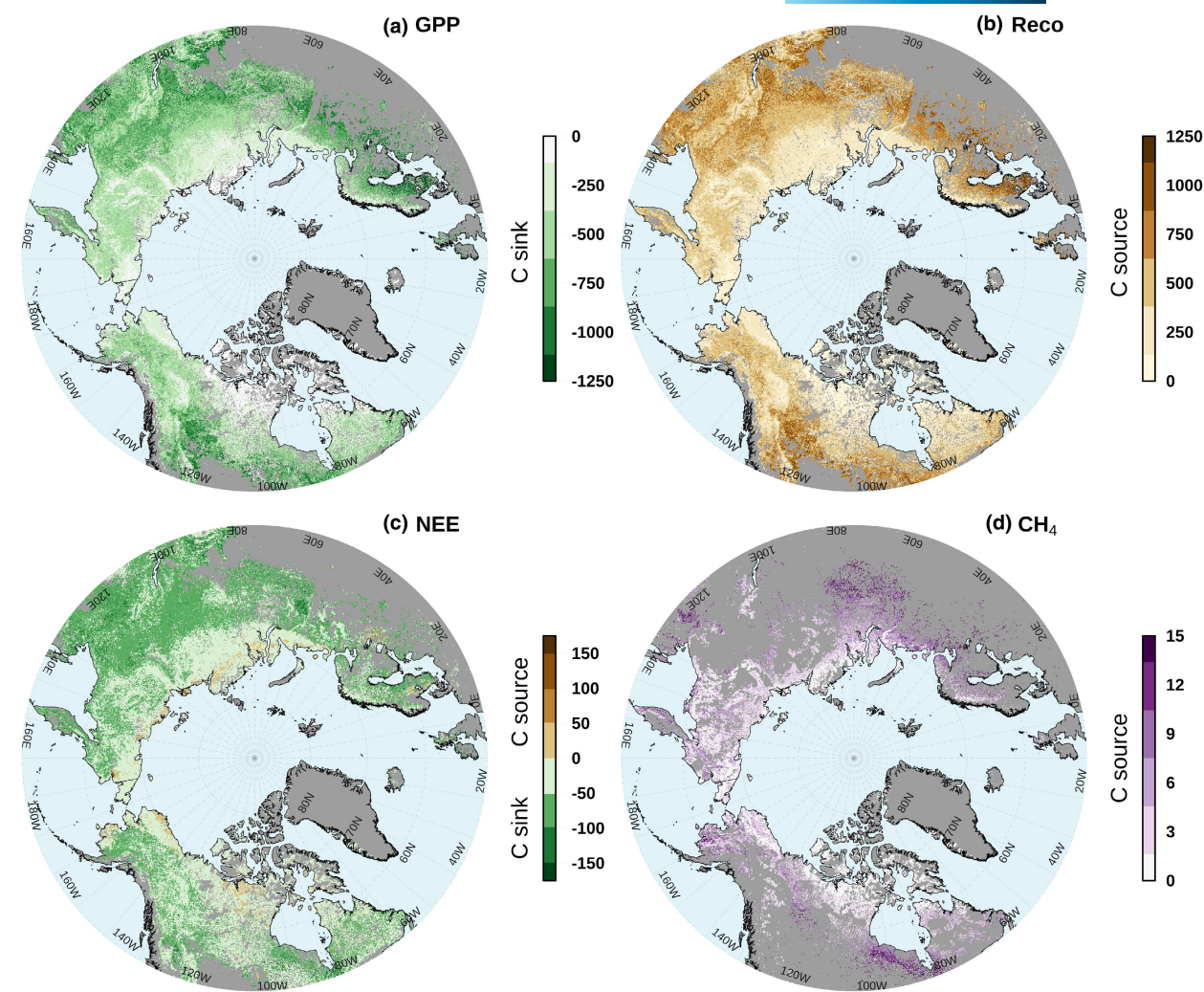


**FIGURE 4** Average annual carbon flux (all units  $\text{g m}^{-2} \text{ year}^{-1}$ ) across the Arctic-boreal domain from 2003 to 2015 as informed by daily 1-km TCFM-Arctic simulations: (a) GPP; (b)  $R_{\text{eco}}$ ; (c) NEE; (d) tundra and boreal wetland  $\text{CH}_4$  emissions with TWI masking.

### 3.3 | Regional NECB emission status

The TCFM-Arctic NECB for the tundra and boreal wetland regions (terrestrial NEE plus wetland  $\text{CH}_4$  emissions) averaged  $-9 \text{ Tg C year}^{-1}$  and  $-246 \text{ Tg C year}^{-1}$ , respectively, over the 2003–2015 period (Table 1). For this study, lands classified as boreal forests and boreal grasslands/shrublands were considered to have non-hydric soil status and therefore non- $\text{CH}_4$  emitting surfaces. Altogether, the Arctic-boreal terrestrial NECB was  $-566 \text{ Tg C year}^{-1}$  for tundra, boreal forest and boreal wetlands, and  $-815 \text{ Tg C year}^{-1}$  when also including boreal grassland/shrublands (Figure 6). Adding in estimates of annual aquatic  $\text{CH}_4$  emissions from open water bodies across the tundra and boreal zone (Johnson et al., 2021, 2022; totaling  $5.3 \text{ Tg C-CH}_4 \text{ year}^{-1}$ ), our estimate of regional  $\text{CH}_4$  uptake ( $-3.9 \text{ Tg C-CH}_4 \text{ year}^{-1}$ ), and regional emissions of  $\text{CO}_2$ ,  $\text{CH}_4$  from fire (average of  $170 \text{ Tg C year}^{-1}$ , based on van Wees et al., 2022), modified the NECB sink status by 21% (totaling  $-640 \text{ Tg C year}^{-1}$ ). Overall, the Eurasian boreal forest region had the largest NECB sink ( $\sim -199 \text{ Tg C year}^{-1}$ ).

## 4 | DISCUSSION

### 4.1 | TCFM-Arctic simulations of eddy covariance tower flux

This study investigates recent (years 2003–2015) changes in Arctic-boreal carbon budgets using flux observations obtained from high-latitude EC tower sites and a 13-year record of daily 1-km resolution NEE, GPP,  $R_{\text{eco}}$ , and  $\text{CH}_4$  simulations from TCFM-Arctic. The resulting model RMSE uncertainty for NEE at high-latitude flux tower sites is an improvement over a previous pan-Arctic model analysis (Watts, Kimball, Parmentier, et al., 2014), and a global assessment of the SMAP L4\_C product (Jones et al., 2017). The RMSE uncertainty for  $\text{CH}_4$  is comparable with values reported in other studies (Watts, Kimball, Bartsch, et al., 2014; Watts, Kimball, Parmentier, et al., 2014), however we acknowledge a bias toward underestimating terrestrial  $\text{CH}_4$  emissions at EC sites dominated by boreal wetlands and graminoid/sedge/shrub tundra (an across-site median underestimate of 25%). Although coarser reanalysis inputs can track regional moisture status

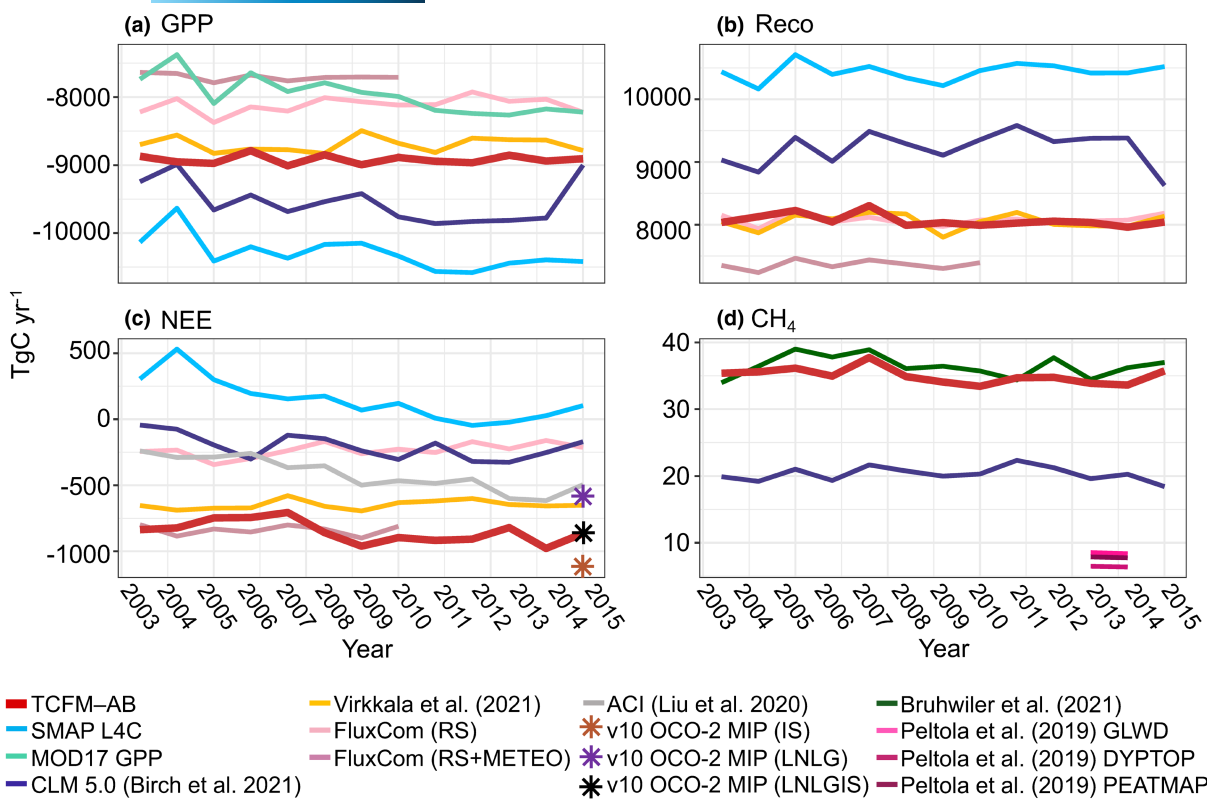


**FIGURE 5** Comparisons of total annual fluxes across the full Arctic-boreal domain for years 2003–2015, estimated from the TCFM-Arctic and other models: The satellite-informed SMAP L4C flux product (Kimball et al., 2012); statistically upscaled CO<sub>2</sub> estimates from FluxCom (Jung et al., 2020; RS and RS+METEO) and Virkkala et al. (2021); an arctic variant of the Community Land Model version 5 (CLM 5; Birch et al., 2021); results from six atmospheric CO<sub>2</sub> inversions (ACI; Liu et al., 2020); v10 Orbiting Carbon Observatory inversion IS, LNGLG, and LNGLG experiment results (OCO-2 MIP; Byrne, Baker, Baker, et al., 2022; Byrne, Liu, et al., 2022); statistically upscaled CH<sub>4</sub> estimates from Peltola et al. (2019); CarbonTracker-CH<sub>4</sub> from Bruhwiler et al. (2014). Annual flux budgets are shown for (a) GPP, (b)  $R_{\text{eco}}$ , (c) NEE, and (d) CH<sub>4</sub>. Negative values of GPP indicate uptake of CO<sub>2</sub> from the atmosphere. Negative values of NEE indicate net carbon sink (where the magnitude of GPP >  $R_{\text{eco}}$ ).

reasonably well, they are unable to identify more localized areas of wetness or dryness (Yi et al., 2011), which would lead to higher uncertainties in estimated fluxes especially in soil respiration and CH<sub>4</sub> modules. We also recognize that under very wet conditions it is possible that some land surfaces in boreal forests and grassland/shrub-lands might have a CH<sub>4</sub> emitting status, which we did not account for in our model. Additionally, TCFM-Arctic does not currently track CH<sub>4</sub> uptake activity that may exist under drier surface conditions, especially in shrub-dominated environments (Kuhn et al., 2021).

Although TCFM-Arctic was able to capture most of the temporal variability observed in the tower EC records, it was unable to account for episodic emissions during spring thaw—when gasses trapped in frozen soils are released following surface ice and snow melt—and episodic releases of CO<sub>2</sub> and CH<sub>4</sub> from soil pore spaces during the autumn freeze (e.g., Mastepanov et al., 2008; Raz-Yaseef et al., 2017). This episodic activity appears more often in environments affected by near-surface permafrost. Because of this, TCFM-Arctic (as with other models, see Byrne, Liu, et al., 2022) is likely underrepresenting regional CO<sub>2</sub> and CH<sub>4</sub> emissions during spring and autumn periods across the tundra-dominated continuous permafrost zone (Arndt et al., 2019; Watts et al., 2021). Based on our comparisons with the EC tower records, TCFM-Arctic may be missing up to 78% (CO<sub>2</sub>) and 40% (CH<sub>4</sub>) of the episodic emissions from tundra environments

during the shoulder seasons, which is considerable especially since field studies in northern Alaska (Arndt et al., 2020; Raz-Yaseef et al., 2017) have found, at some locations, the amount of built-up CO<sub>2</sub> released from soil during the spring snowmelt period can offset up to 41%–46% of summer CO<sub>2</sub> uptake. Additionally, regional studies (Byrne, Liu, et al., 2022; Commane et al., 2017; Schiferl et al., 2022) have documented a shift toward more respiration in autumn, that might increasingly offset summer GPP. This emphasizes the need for models to effectively account for the mechanisms driving shoulder season emissions. Including multi-layer heat transfer and permafrost hydrology modules within the TCFM-Arctic framework would likely improve shoulder season emission estimates, but at the expense of greater model complexity and computational burden.

## 4.2 | Regional net ecosystem CO<sub>2</sub> exchange and CH<sub>4</sub> flux budgets

### 4.2.1 | Terrestrial CO<sub>2</sub>

Our model-based analysis indicates that for the 2003–2015 study period the Arctic-boreal region, as a whole, was a NEE sink ( $-850 \text{ Tg CO}_2 \text{-C year}^{-1}$ ), with an associated uncertainty of  $\pm 744\text{--}1138 \text{ Tg CO}_2 \text{-C year}^{-1}$ ). This

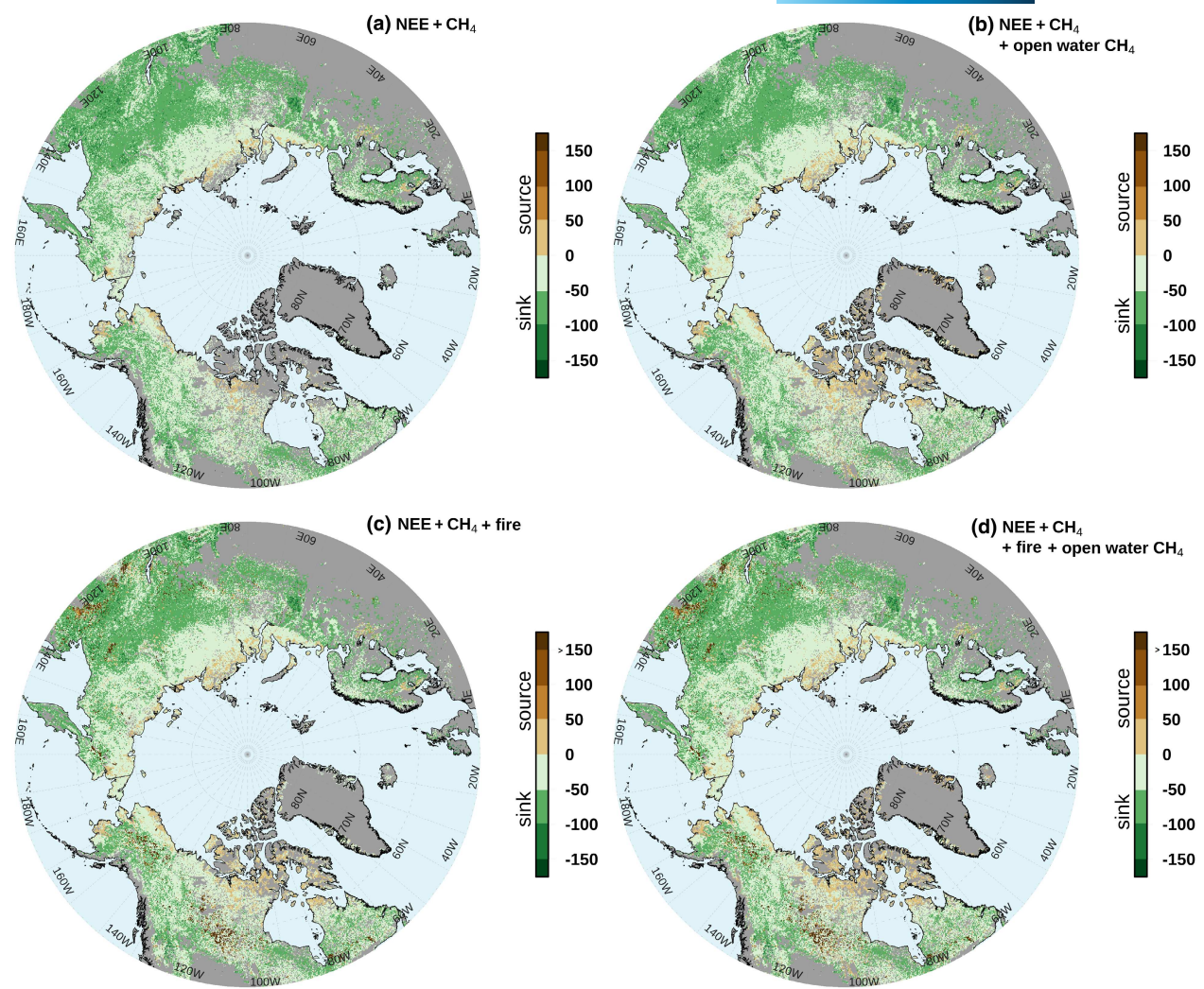


**FIGURE 6** Maps of (a) average annual NEE + terrestrial CH<sub>4</sub> from 2003 to 2015; (b) NEE + terrestrial CH<sub>4</sub> + aquatic open water CH<sub>4</sub> sources; (c) NEE + terrestrial CH<sub>4</sub> + carbon sources from fire; (d) NEE + terrestrial CH<sub>4</sub> + aquatic open water CH<sub>4</sub> + fire. Units are in g C m<sup>-2</sup> year<sup>-1</sup>.

finding is closely aligned with atmospheric budgets from the OCO-2 MIP LNLGIS experiment (Byrne, Baker, et al., 2022; Byrne, Liu, et al., 2022), which used satellite-retrieved column-averaged dry-air atmospheric mole fractions (providing finer-spatial tracking of CO<sub>2</sub>), in addition to in situ CO<sub>2</sub> measurements. For bottom-up models, our results were most closely within the range of two EC tower and remote-sensing informed machine learning approaches—FluxCom RS + METEO (Jung et al., 2020) and Virkkala et al. (2021).

We found boreal systems (forests, wetlands, and shrublands/grasslands) accounted for nearly all (98%) of the NEE sink, with the remainder provided by tundra. We also found some evidence of an increasing annual NEE sink within the Eurasian boreal, which has also been observed elsewhere (Welp et al., 2016). Eurasia contributed to a majority (74%) of the boreal NEE sink, and the largest CO<sub>2</sub> sink by area was observed in the larch-dominated East Siberian Taiga. Although the geographically extensive Eastern Siberian Taiga remains largely underrepresented by EC tower monitoring sites (Pallandt et al., 2022), this region has been identified as an important, perhaps increasing, carbon sink (Byrne, Liu, et al., 2022; Lin et al., 2020; Sato et al., 2016;

Schulze, 2006). However, elevated fire activity here in recent years (post-2015) (Veraverbeke et al., 2021) might now be offsetting more of the carbon uptake. Further study of the East Siberian Taiga should be a high priority for future research.

Over the study period, we observed contrasting changes in Eurasian versus North American boreal NEE status, as indicated by the TCFM-Arctic simulations. The Eurasian boreal zone showed a strong significant increase in annual NEE sink, whereas the North American boreal showed the opposite pattern (a weakening NEE sink) primarily driven by a decrease in GPP. The strong contrast in NEE activity between Eurasia and North America has been reported elsewhere (Bi et al., 2013; Byrne, Liu, et al., 2022; Lin et al., 2020; Tagesson et al., 2020). Much of this difference is likely driven by more frequent and severe wildfire activity in North America relative to Eurasia (Wang et al., 2020; Zhao et al., 2021), and sustained periods of drought leading to tree mortality (Berner & Goetz, 2022; Girardin et al., 2016; Peng et al., 2011; Rogers et al., 2018; Sulla-Menashe et al., 2018). In northern Canada, loss of NEE uptake has also been reported due to wetland expansion

following rapid permafrost thaw, and the subsequent loss of established forests (Helbig et al., 2017).

In contrast to the boreal zone, a majority of the models evaluated here (including TCFM-Arctic) indicated the tundra domain as being, on average, neutral or a small source for NEE. However, adjusting the TCFM-Arctic tundra NEE budget to account for a potentially large underestimation of episodic  $\text{CO}_2$  emissions during spring and autumn shoulder seasons (Arndt et al., 2020; Byrne, Baker, et al., 2022; Byrne, Liu, et al., 2022; Commane et al., 2017; Liu et al., 2022; Schiferl et al., 2022) would shift tundra NEE status more toward an annual carbon source.

Overall, our estimate of NEE sink activity for boreal forests and wetlands ( $\sim 585 \text{Tg CO}_2\text{-C}$ ) is close to an inventory-based estimate of the annual boreal forest carbon sink ( $\sim 500 \text{Tg CO}_2\text{-C}$ ; Pan et al., 2011). Our estimate of boreal forest NEE ( $-311 \pm 405 \text{Tg CO}_2\text{-Cyear}^{-1}$ ) is also within the range of the other evaluated bottom-up models ( $-641$  to  $47 \text{Tg CO}_2\text{-Cyear}^{-1}$ ) and atmospheric inversions ( $-459$  to  $-81 \text{g CO}_2\text{-Cyear}^{-1}$ ). In contrast, for the boreal wetlands, the TCFM-Arctic simulations indicated a stronger NEE sink ( $-274 \pm 255 \text{Tg CO}_2\text{-Cyear}^{-1}$ ) relative to the other bottom-up models ( $-161$  to  $95 \text{Tg CO}_2\text{-Cyear}^{-1}$ ) and inversion results ( $-181$  to  $-103 \text{Tg CO}_2\text{-Cyear}^{-1}$ ). That the NEE sink strength we observed for boreal wetlands was nearly on par with the forest sink activity was unexpected. However, some field observations have also shown a negligible difference between NEE sinks in boreal forests and boreal wetland systems intermixed with trees (Helbig et al., 2017). We acknowledge that the strength of the boreal wetland sink may largely vary across the region, with local hydrology being a key factor. Field studies indicate that boreal wetlands, including bogs and fens, can shift between strong annual NEE sink (when soils remain very wet) and source (when soils are warm and less wet) (e.g., Euskirchen et al., 2014; Laine et al., 2019; Olefeldt et al., 2017; Rinne et al., 2020; Schulze et al., 1999) depending on water table depth and soil wetness.

In this study, we identified the grassland/shrubland class as contributing a large source of NEE uncertainty for the boreal zone. The exact characteristics of this class are relatively unknown, though within North America, shrubland and grassland communities tend to establish after severe fire disturbances in forests, particularly in warmer and drier regions (Berner & Goetz, 2022). Our TCFM-Arctic estimate of the NEE sink for shrublands/grasslands was  $-249 \text{Tg CO}_2\text{-Cyear}^{-1}$  ( $-255$  to  $85 \text{Tg CO}_2\text{-Cyear}^{-1}$  in the other models), slightly lower than the boreal wetland class. Because reference EC data explicitly representing this vegetation class (which tends to be more mesic relative to wetlands) were not available for model calibration and uncertainty assessments, it is possible TCFM-Arctic is overestimating NEE sink activity, but new EC observations specific to shrublands/grasslands are needed for further verification.

#### 4.2.2 | Wetland $\text{CH}_4$

We estimated an annual loss of  $35 \text{Tg CH}_4\text{-C}$  for the Arctic-boreal domain, with tundra contributing 18% of the emissions compared

with 82% from boreal wetlands. Approximately 54% and 28% of respective emissions were from boreal wetlands in Eurasia and North America. In our model, we detected a slight increase in  $\text{CH}_4$  emissions from tundra regions in Eurasia (which was also reported in Thompson et al., 2017), possibly stemming from a period of warming and wetting. However, this change was countered by a decrease in North America tundra emissions. We did not detect significant changes in  $\text{CH}_4$  emissions for boreal wetlands, which concurs with a recent report (Bruhwiler et al., 2021).

Even though TCFM-Arctic underestimated  $\text{CH}_4$  emissions at boreal EC sites, for the full Arctic-boreal region our estimates are higher than the other bottom-up assessments directly evaluated in this study (i.e., Birch et al., 2021; Peltola et al., 2019;  $6\text{--}20 \text{Tg CH}_4\text{-Cyear}^{-1}$ ). Our results are slightly above the range of optimized  $\text{CH}_4$  emission estimates ( $9\text{--}22 \text{Tg CH}_4\text{-Cyear}^{-1}$ ) from bottom-up informed high-resolution inversion models for the pan-Arctic domain (see Tan et al., 2016) which focused on lands  $\geq 60^\circ$  (compared with  $\geq 50^\circ$  in our study). However, our results were very similar to the atmosphere-informed CarbonTracker- $\text{CH}_4$  records examined in this analysis. As has been reported elsewhere (Melton et al., 2013), much of the differences in bottom-up estimates (and inverse estimates informed by priors from bottom-up models) stem from how  $\text{CH}_4$  emitting regions and wetland extent are identified (e.g., Melton et al., 2013; Zhang et al., 2017). As with most models, our accounting of  $\text{CH}_4$  was terrestrially focused and did not provide estimates for rivers (see Stanley et al., 2022), open water lakes and ponds.

#### 4.2.3 | Regional NECB

Our estimate of Arctic-boreal NECB, when considering terrestrial NEE and  $\text{CH}_4$  emissions (and not factoring in  $\text{CH}_4$  uptake) was  $-815 \text{Tg Cyear}^{-1}$  with boreal wetland and tundra  $\text{CH}_4$  offsetting the NEE sink by only 4%. Accounting for aquatic  $\text{CH}_4$  emissions from open water (using recent estimates from Johnson et al., 2021, 2022), and emissions from fire (van Wees et al., 2022), reduced the NECB sink status by 21%.

Although we found the full region to be a NECB sink (based on average NECB, with a large range of uncertainty), we also observed NECB local source areas. These source areas included portions of the Alaskan Interior (primarily within burned landscapes), Yukon-Kuskokwim Delta (YKD), and North Slope coastal regions where  $\text{CH}_4$  emissions from wetlands and open water contributed to the net carbon source status. In Canada, NECB source areas included Nunavut, the Northwest Territories, northern regions of Saskatchewan and Manitoba, and northwest Quebec which have experienced substantial drought and fire disturbance (Whitman et al., 2019; Zhao et al., 2021). In Siberia, NECB source occurred primarily across the tundra, driven by  $R_{\text{eco}}$  outpacing GPP, and within the southern boreal zone which has been impacted by drought and fire (Sun et al., 2021; Veraverbeke et al., 2021).

We acknowledge a very large uncertainty in high-latitude aquatic emission budgets (for  $\text{CH}_4$  and  $\text{CO}_2$ ), which was not included in our

budget estimates; Billet et al., 2015; Webb et al., 2019); this may contribute to substantial underestimation of regional carbon emissions. Additionally, small ponds are largely unaccounted for in water body maps and are not well represented in  $\text{CO}_2$  and  $\text{CH}_4$  emissions budgets. Not accounting for emissions from small ponds has been shown to result in substantial overestimation of net carbon uptake in tundra (Beckebanze et al., 2022). Furthermore, we recognize possibly substantial  $\text{CO}_2$  and  $\text{CH}_4$  emission contributions stemming from rapidly thawing and collapsing permafrost landscapes and the release of older carbon from deeper soil reservoirs (Miner et al., 2022; Turetsky et al., 2019), which remains largely unaccounted for by EC towers, ecosystem models, and regional carbon budgets.

## 5 | CONCLUSIONS AND IMPLICATIONS FOR FUTURE WORK

Our study indicates that the Arctic-boreal region contributed to substantial NEE sink activity over the 2003–2015 period, with most of the  $\text{CO}_2$  sink driven by forests across the Siberian boreal zone. Conversely, the tundra region ranged from neutral to a small NEE source and, in many areas, was a stronger NECB source when considering  $\text{CH}_4$  and fire emissions. Accounting for  $\text{CH}_4$  and fire emissions in the boreal region resulted in a NECB source in some wetland complexes (e.g., the Alaska YKD) and in landscapes disturbed by drought and wildfire.

As with this assessment, other reports have highlighted the importance of the boreal  $\text{CO}_2$  sink—perhaps on par with the tropical forest sink (Tagesson et al., 2020)—and indicate a large unrealized potential of boreal forests to sequester additional carbon (approximately 46 PgC total) through protection and restoration (Walker et al., 2022). Although some studies estimate that this NEE sink will continue to increase through 2100 (Holmberg et al., 2019; White et al., 2001), it is very likely that an increase in fire activity, already observed in more recent years, will threaten historic carbon gains (Walker et al., 2019). Fire disturbances are often identified as the primary driver of changing carbon budgets across the Arctic-boreal region (Bond-Lamberty et al., 2007), with added effects from extreme water stress—drought and inundation (Helbig et al., 2017; Peng et al., 2011). Fire activity in permafrost systems is also an added threat because it can accelerate soil thaw, and the release of older carbon (Schädel et al., 2016; Turetsky et al., 2019). Given the considerable boreal carbon sink observed in this study, and the threat of increased disturbance reducing the forest sink, we recommend the urgent protection of highly productive boreal regions through targeted fire management and limits to human disturbances (Phillips et al., 2022; Shvetsov et al., 2021).

Although we observed similarities in reported NEE between TCFM-Arctic and other bottom-up models (especially those calibrated for high-latitude regions), for some models there was substantial disagreement in the estimated sign and magnitude of NEE. Discrepancies in modeled carbon budgets have also been

identified elsewhere (e.g., Fisher et al., 2014; McGuire et al., 2012; Melton et al., 2013; Natali et al., 2019; Virkkala et al., 2021), and this issue remains problematic in the science community's attempt to reconcile the status and trajectory of high-latitude ecosystem carbon budgets (Euskirchen et al., 2022). However, we did find the regional TCFM-Arctic estimates to align closely with those from top-down models (i.e., especially CarbonTracker- $\text{CH}_4$  and OCO-2 MIP LNLGIS), providing some consensus. Moving forward, coordinated efforts between bottom-up and top-down (atmospheric) communities to identify key model assumptions and sources of agreement and uncertainty—including the representation of soil hydrology and its influence on uncertainty (de Vrese et al., 2022)—must be prioritized to close the gap in Arctic-boreal carbon budget estimates. Increasing atmospheric sampling (e.g., flasks, tall towers, airborne) networks within high-priority Arctic-boreal sub-regions, while also leveraging trace gas observations from satellites, would allow for top-down versus bottom-up model comparisons at more local scales (Lauvaux et al., 2012; Parazoo et al., 2016; Schuh et al., 2013).

At present, spaceborne monitoring systems are unable to track changing emission contributions in winter (Parazoo et al., 2016), which is a period of substantial carbon emission (Natali et al., 2019; Watts et al., 2021; this study), but are increasingly able to monitor changing atmospheric  $\text{CO}_2$  and  $\text{CH}_4$  concentrations in shoulder and summer seasons at relatively fine spatial resolutions (1–10 km), improving the detection of regional shifts in the NECB (Byrne, Liu, et al., 2022; Miner et al., 2022). Investments in future satellite missions that provide the capacity for year-round detection of  $\text{CO}_2$  and  $\text{CH}_4$  (e.g., such as the planned Methane Remote Sensing Lidar Mission, MERLIN; Ehert et al., 2017) should be a high-priority, as well as investments in combined active and passive microwave spaceborne sensors for finer-resolution, year-round detection of soil thermal and moisture states (building upon lessons learned from NASA's SMAP mission). However, even with improvements in spaceborne detection and inversion modeling, bottom-up approaches (i.e., in situ monitoring sites and model simulations) will be needed to diagnose local trajectories of change and to identify how various ecosystem components and feedbacks are amplifying or mitigating observed changes in the carbon cycle (Schuur & Mack, 2018).

Based on our analysis, we identify a pressing need for new investments in local EC tower and regional atmospheric monitoring networks that target: (1) larch-dominated ecosystems, especially those in eastern Siberia; (2) poorly characterized boreal grasslands/shrublands; (3) boreal and tundra landscapes undergoing severe ground thaw following fires and thermokarst; (4) aquatic ecosystems, including small ponds (focusing on  $\text{CH}_4$  and  $\text{CO}_2$  emissions). We also emphasize an immediate need for continued investments that support, and expand, year-round EC monitoring at all tower sites across the domain. Acquiring these observations is crucial in determining the primary drivers of uncertainties in bottom-up and top-down models, and the overall status and trajectory of this rapidly changing region.

## ACKNOWLEDGEMENTS

This study was part of the NASA Arctic-Boreal Vulnerability Experiment (ABOVE). J.D.W. and M.F. were supported through funding from the NASA New Investigator Program (80NSSC18K0770) and Future Investigators in NASA Earth and Space Science and Technology (FINESST; 19-EARTH20-0105). J.D.W. and J.S.K. were supported through funding from Phase 1 of NASA ABOVE (NNX15AT74A). M.S.J. acknowledges funding from NASA's Interdisciplinary Research for Earth Science (IDS) Program and the NASA Terrestrial Ecology and Tropospheric Composition Programs. S.J.G. acknowledges NASA ABOVE grant 80NSSC19M0113. A.V. and J.D.W. acknowledge support from the Gordon and Betty Moore Foundation (8414). Contributions by J.K. were supported by NSF grant 1203583. B.B.'s research was carried out at the Jet Propulsion Laboratory, California Institute of Technology, under a contract with the National Aeronautics and Space Administration (80NM0018D004). Resources supporting this work were provided by the NASA High-End Computing Program through the NASA Center for Climate Simulation at Goddard Space Flight Center. Finally, we acknowledge data contributions from Rikie Suzuki and support from the NASA ABOVE community and our international collaborators.

## CONFLICT OF INTEREST

The authors have no conflict of interest to declare.

## DATA AVAILABILITY STATEMENT

The geospatial files for TCFM-Arctic are available through <https://doi.org/10.3334/ORNLDAC/2121>. The eddy covariance data were obtained from the European Fluxes Database (<http://www.europe-fuxdata.eu/home>), from the Ameriflux Database (<http://ameriflux.lbl.gov/>), from AsiaFlux (<https://www.asiaflux.net/>), from <https://data.g-e-m.dk>, and from the ABCFlux database ([https://daac.ornl.gov/ABOVE/guides/Arctic\\_Boreal\\_CO2\\_Flux.html](https://daac.ornl.gov/ABOVE/guides/Arctic_Boreal_CO2_Flux.html)). We also received flux information directly from tower PIs, as indicated in Table S1. All original data shown in Table S1 can be found through <https://doi.org/10.3334/ORNLDAC/2121>. Additionally, the winter respiration fluxes we used for model calibration are available through <https://doi.org/10.3334/ORNLDAC/1692>.

## ORCID

Jennifer D. Watts  <https://orcid.org/0000-0001-7207-8999>

Luke D. Schiferl  <https://orcid.org/0000-0002-5047-2490>

Torben Tagesson  <https://orcid.org/0000-0003-3011-1775>

## REFERENCES

Abbott, B. W., Jones, J. B., Schuur, E. A. G., Chapin, F. S., III, Bowden, W. B., & Zimov, S. (2016). Biomass offsets little or none of permafrost carbon release from soils, streams, and wildfire: An expert assessment. *Environmental Research Letters*, 11, 034014.

Arndt, K. A., Lipson, D. A., Hashemi, J., Oechel, W. C., & Zona, D. (2020). Snow melt stimulates ecosystem respiration in Arctic ecosystems. *Global Change Biology*, 26, 1–10.

Arndt, K. A., Oechel, W. C., Goodrich, J. P., Bailey, B. A., Kalhori, A., Hashemi, J., Sweeney, C., & Zona, D. (2019). Sensitivity of methane emissions to later soil freezing in Arctic tundra ecosystems. *JGR: Biogeosciences*, 124, 2595–2609.

Balcombe, P., Speirs, J. F., Brandon, N. P., & Hawkes, A. D. (2018). Methane emissions: Choosing the right climate metric and time horizon. *Environmental Science: Processes & Impacts*, 20, 1323–1339. <https://doi.org/10.1029/C8EM00414E>

Baldocchi, D. (2020). How eddy covariance flux measurements have contributed to our understanding of global change biology. *Global Change Biology*, 26, 242–260. <https://doi.org/10.1111/gcb.14807>

Baldocchi, D., Falge, E., Gu, L., Olson, R., Hollinger, D., Running, S., Anthoni, P., Bernhofer, C., Davis, K., Evans, R., Fuentes, J., Goldstein, A., Katul, G., Law, B., Lee, X., Malhi, Y., Meyers, T., Munger, W., Oechel, W., ... Wofsy, S. (2001). FLUXNET: A new tool to study the temporal and spatial variability of ecosystem-scale carbon dioxide, water vapor, and energy flux densities. *Bulletin of the American Meteorological Society*, 82, 2415–2434.

Baldocchi, D., & Koteen, L. (2012). Methane flux measurements, new opportunities for FLUXNET. *FluxLetter*, 4, 1–15.

Ballantyne, A. P., Liu, Z., Anderegg, W. R. L., Yu, Z., Stoy, P., Poulter, B., Vanderwall, J., Watts, J. D., Kelsey, K., & Neff, J. (2021). Reconciling carbon-cycle processes from ecosystem to global scales. *Frontiers in Ecology and the Environment*, 19, 57–65. <https://doi.org/10.1002/fee.2296>

Beckebanze, L., Rehder, Z., Holl, D., Wille, C., Mirbach, C., & Kutzbach, L. (2022). Ignoring carbon emissions from thermokarst ponds results in overestimation of tundra net carbon uptake. *Biogeosciences*, 19, 1225–1244.

Belshe, E. F., Schuur, E. A. G., & Bolker, B. M. (2013). Tundra ecosystems observed to be CO<sub>2</sub> sources due to differential amplification of the carbon cycle. *Ecology Letters*, 16, 1307–1315.

Berner, L. T., & Goetz, S. J. (2022). Satellite observations document trends consistent with a boreal forest biome shift. *Global Change Biology*, 10, 3275–3292.

Bi, J., Xu, L., Samanta, A., Zhu, Z., & Myneni, R. (2013). Divergent Arctic-boreal vegetation changes between North America and Eurasia over the past 30 years. *Remote Sensing*, 5, 2093–2112.

Billet, M. F., Garnett, M. H., & Dinsmore, K. J. (2015). Should aquatic CO<sub>2</sub> evasion be included in contemporary carbon budgets for peatland ecosystems. *Ecosystems*, 18, 471–480.

Birch, L., Schwalm, C. R., Natali, S., Lombardozzi, D., Keppel-Aleks, G., Watts, J. D., Lin, X., Zona, D., Oechel, W., Sachs, T., Black, T. A., & Rogers, B. M. (2021). Addressing biases in Arctic-boreal carbon cycling in the community land model version 5. *Geoscientific Model Development*, 14, 3361–3382.

Biskaborn, B. K., Smith, S. L., Noetzli, J., Matthes, H., Vieira, G., Streletskiy, D. A., Schoeneich, P., Romanovsky, V. E., Lewkowicz, A. G., Abramov, A., Allard, M., Boike, J., Cable, W. L., Christiansen, H. H., Delaloye, R., Diekmann, B., Drotzov, D., Etzelmüller, B., Grosse, G., ... Lantuit, H. (2019). Permafrost is warming at a global scale. *Nature Communications*, 10, 264.

Bond-Lamberty, B., Peckham, S. D., Ahl, D. E., & Gower, S. T. (2007). Fire as the dominant driver of Central Canadian boreal forest carbon balance. *Nature*, 450, 89–92.

Box, J. E., Colgan, W. T., Christensen, T. R., Schmidt, N. M., Lund, M., Parmentier, F.-J. W., Brown, R., Bhatt, U. S., Euskirchen, E. S., & Romanovsky, V. E. (2019). Key indicators of Arctic climate change: 1971–2017. *Environmental Research Letters*, 14, 045010.

Bradshaw, C. J. A., & Warkentin, I. G. (2015). Global estimates of boreal forest carbon stocks and flux. *Global and Planetary Change*, 128, 24–30.

Bronaugh, D., & Werner, A. (2019). *Zhang + Yue-Pilon Trends Package*, version 0.10-1.1. <https://CRAN.R-project.org/package=zyp>

Brown, J., Ferrians, O., Heginbottom, J. A., & Melnikov, E. (2002). *Circum-Arctic map of permafrost and ground-ice conditions*, version 2. NSIDC: National Snow and Ice Data Center.

Bruhwiler, L., Dlugokencky, E., Masarie, K., Ishizawa, M., Andrews, A., Miller, J., Sweeney, C., Tans, P., & Worthy, D. (2014). CarbonTracker-CH<sub>4</sub>: An assimilation system for estimating emissions of atmospheric methane. *Atmospheric Chemistry and Physics*, 14, 8269–8293.

Bruhwiler, L., Parmentier, F.-J. W., Crill, P., Leonard, M., & Palmer, P. I. (2021). The Arctic carbon cycle and its response to changing climate. *Current Climate Change Reports*, 7, 14–34.

Byrne, B., Baker, D. F., Basu, S., Bertolacci, M., Bowman, K. W., Carroll, D., Chatterjee, A., Chevallier, F., Ciais, P., Cressie, N., Crisp, D., Crowell, S., Deng, F., Deng, Z., Deutscher, N. M., Dubey, M., Feng, S., Garcia, O., Griffith, D. W. T., ... Zeng, N. (2022). National CO<sub>2</sub> budgets (2015–2022) inferred from atmospheric CO<sub>2</sub> observations in support of the global Stocktake. *Earth System Science Earth System Science Data Discussions*. <https://doi.org/10.5194/essd-2022-213>

Byrne, B., Liu, J., Yi, Y., Chatterjee, A., Basu, S., Cheng, R., Doughty, R., Chevallier, F., Bowman, K. W., Parazoo, N. C., Crisp, D., Li, X., Xiao, J., Sitch, S., Guenet, B., Deng, F., Johnson, M. S., Philip, S., McGuire, P. C., & Miller, C. E. (2022). Multi-year observations reveal a larger than expected autumn respiration signal across Northeast Eurasia. *Biogeosciences*, 19, 4779–4799.

CAVM Team. (2003). *Circumpolar Arctic Vegetation Map*. (1:7,500,000 scale), Conservation of Flora and Fauna (CAFF) Map. No. 1. Fish and Wildlife Service, Anchorage, Alaska. ISBN: 0-9767525-0-6.

Celis, G., Pallandt, M., & Goeckede, M. (2020). Carbon flux sites mapping tool. Arctic Data Center. <https://cosima.nceas.ucsb.edu/carbo-n-flux-sites/>

Chadburn, S. W., Krinner, G., Porada, P., Bartsch, A., Beer, C., Marchesini, L. B., Boike, J., Ekici, A., Elberling, B., Friborg, T., Hugelius, G., Johansson, M., Kuhry, P., Kutzbach, L., Langer, M., Lund, M., Parmentier, F.-J. W., Peng, S., Van Huissteden, K., ... Burke, E. J. (2017). Carbon stocks and fluxes in the high latitudes: Using site-level data to evaluate Earth system models. *Biogeosciences*, 14, 5143–5169.

Christensen, T. R., Rysgaard, S., Bendtsen, J., Brent, E., Glud, R. N., van Huissteden, J., Parmentier, F. J. W., Sachs, T., & Vonk, J. E. (2017). Arctic carbon cycling. In *Snow, water, ice and permafrost in the Arctic. Arctic Monitoring and Assessment Programme (AMAP)* (pp. 203–218). ISBN 978-82-7971-101-8.

Chylek, P., Folland, C., Klett, J. D., Wang, M., Hengartner, N., Lesins, G., & Dubey, M. K. (2022). Annual mean Arctic amplification 1970–2020: Observed and simulated by CMIP6 climate models. *Geophysical Research Letters*, 49, e2022GL099371. <https://doi.org/10.1029/2022GL099371>

Ciais, P., Canadell, J. G., Luyssaert, S., Chevallier, F., Shvidenko, A., Poussi, Z., Jonas, M., Peylin, P., King, A. W., Schulze, E.-D., Piao, S., Rodenbeck, C., Peters, W., & Breon, F.-M. (2010). Can we reconcile atmospheric estimates of the northern terrestrial carbon link with land-based accounting? *Current Opinion in Environmental Sustainability*, 2, 225–230.

Commane, R., Lindaas, J., Benmergui, J., Luus, K. A., Chang, R. Y.-W., Daube, B. C., Euskirchen, E. S., Henderson, J. M., Karion, A., Miller, J. B., Miller, S. M., Parazoo, N. C., Randerson, J. T., Sweeney, C., Tans, P., Thoning, K., Veraverbeke, S., Miller, C. E., & Wofsy, S. C. (2017). Carbon dioxide sources from Alaska driven by increasingly early winter respiration from Arctic tundra. *Proceedings of the National Academy of Sciences of the United States of America*, 114, 5361–5366.

de Vrese, P., Georgievski, G., Rouco, J. F. G., Notz, D., Stacke, T., Steinert, N. J., Wilkenskjeld, S., & Brovkin, V. (2022). Representation of soil hydrology in permafrost regions may explain a large part of inter-model spread in simulated Arctic and subarctic climate. *The Cryosphere Discussions*. <https://doi.org/10.5194/tc-2022-150>

Dinerstein, E., Olson, D., Joshi, A., Vynne, C., Burgess, N. D., Wikramanayake, E., Hahn, N., Palminteri, S., Hedao, P., Noss, R., & Hansen, M. (2017). An ecoregion-based approach to protecting half the terrestrial realm. *BioScience*, 67, 534–545.

Ehert, G., Bousquet, P., Pierangelo, C., Alpers, M., Millet, B., Abshire, J. B., Bovensmann, H., Burrows, J. P., Chevallier, F., Ciais, P., Crevoisier, C., Fix, A., Flamant, P., Frankenberger, C., Gibert, F., Heim, B., Heimann, M., Houweling, S., Hubberken, H. W., ... Wirth, M. (2017). MERLIN: A French-German space lidar mission dedicated to atmosphere methane. *Remote Sensing*, 9, 1052.

Euskirchen, E., Edgar, C. W., Turetsky, M. R., Waldrop, M. P., & Harden, J. W. (2014). Differential response of carbon fluxes to climate in three peatland ecosystems that vary in the presence and stability of permafrost. *Journal of Geophysical Research*, 119, 1576–1595.

Euskirchen, E. S., Bret-Harte, M. S., Shaver, G. R., Edgar, C. W., & Romanovsky, V. E. (2017). Long-term release of carbon dioxide from Arctic tundra ecosystems in Alaska. *Ecosystems*, 20, 960–974.

Euskirchen, E. S., Bruhwiler, L. M., Commane, R., Parmentier, F. J. W., Schadel, C., Schuur, E. A. G., & Watts, J. D. (2022). Current knowledge and uncertainties associated with the Arctic greenhouse gas budget. In B. Poulter, J. G. Canadell, D. J. Hayes, & R. L. Thompson (Eds.), *Balancing greenhouse gas budgets* (pp. 159–201). Elsevier.

Fisher, J. B., Sikka, M., Oechel, W. C., Huntzinger, W. C., Melton, D. N., Koven, C. D., Ahlstrom, A., Arain, M. A., Baker, I., Chen, J. M., Ciais, P., Davidson, C., Dietze, M., El-Masri, B., Hayes, D., Huntingford, C., Jain, A. K., Levy, P. E., Lomas, M. R., ... Miller, C. E. (2014). Carbon cycle uncertainty in the Alaskan Arctic. *Biogeosciences*, 11, 4271–4288.

Forster, P., Storelvmo, T., Armour, K., Collins, W., Dufresne, J.-L., Frame, D., Lunt, D. J., Mauritsen, T., Palmer, M. D., Watanabe, M., Wild, M., & Zhang, H. (2021). The Earth's energy budget, climate feedbacks, and climate sensitivity. In V. Masson-Delmotte, P. Zhai, A. Pirani, S. L. Connors, C. Péan, S. Berger, N. Caud, Y. Chen, L. Goldfarb, M. I. Gomis, M. Huang, K. Leitzell, E. Lonnoy, J. B. R. Matthews, T. K. Maycock, T. Waterfield, O. Yelekçi, R. Yu, & B. Zhou (Eds.), *Climate change 2021: The physical science basis. Contribution of Working Group I to the sixth assessment report of the Intergovernmental Panel on Climate Change* (pp. 923–1054). Cambridge University Press. <https://doi.org/10.1017/9781009157896.009>

Fox, A. M., Huntley, B., Lloyd, C. R., Williams, M., & Baxter, R. (2008). Net ecosystem exchange over heterogeneous Arctic tundra: Scaling between chamber and eddy covariance measures. *Global Biogeochemical Cycles*, 22. <https://doi.org/10.1029/2007GB003027>

Friedl, M. A., Sulla-Menashe, D., Tan, B., Schneider, A., Ramankutty, N., Sibley, A., & Huang, X. (2010). MODIS collection 5 global land cover: Algorithm refinements and characterization of new datasets, 2001–2012, collection 5.1 IGBP land cover. Boston University.

Girardin, M. P., Bouriaud, O., Hogg, E. H., Kurz, W., Zimmermann, N. E., Metsaranta, J. M., Jong, R., de Frank, D. C., Esper, J., Büntgen, U., Guo, X. J., & Bhatti, J. (2016). No growth stimulation of Canada's boreal forest under half-century of combined warming and CO<sub>2</sub> fertilization. *Proceedings of the National Academy of Sciences of the United States of America*, 113, E8406–E8414. <https://doi.org/10.1073/pnas.1610156113>

Hartery, S., Commane, R., Lindaas, J., Sweeney, C., Henderson, J., Mountain, M., Steiner, N., McDonald, K., Dinardo, S. J., Miller, C. E., Wofsy, S. C., & Chang, R. Y.-W. (2018). Estimating regional-scale methane flux and budgets using CARVE aircraft measurements over Alaska. *Atmospheric Chemistry and Physics*, 18, 185–202.

Hashemi, J., Zona, D., Arndt, K. A., Kalhori, A., & Oechel, W. C. (2021). Seasonality buffers carbon budget variability across heterogeneous landscapes in Alaskan Arctic tundra. *Environmental Research Letters*, 16, 035008.

Helbig, M., Chasmer, L. E., Desai, A. R., Kljun, N., Quinton, W. L., & Sonnentag, O. (2017). Direct and indirect climate change effects on carbon dioxide fluxes in a thawing boreal forest-wetland landscape. *Global Change Biology*, 23, 3231–3248.

Holmberg, M., Aalto, T., Akujarvi, A., Arslan, A. N., Bergstrom, I., Bottcher, K., Lahtinen, I., Mäkelä, A., Markkanen, T., Minunno, F., Peltoniemi, M., Rankinen, K., & Vihervara, M. F. (2019). Ecosystem services related to carbon cycling—Modeling present and future impacts in boreal forests. *Frontiers in Plant Science*, 10, 343. <https://doi.org/10.3389/fpls.2019.00343>

Hugelius, G., Tarnocai, C., Broll, G., Canadell, J. G., Kuhry, P., & Swanson, D. K. (2013). The northern circumpolar soil carbon database: Spatially distributed datasets of soil coverage and soil carbon storage in the northern permafrost regions. *Earth System Science Data*, 5, 3–13.

Johnson, M. S., Matthews, E., Bastviken, D., Deemer, B., Du, J., & Genovese, V. (2021). Spatiotemporal methane emission from global reservoirs. *Journal of Geophysical Research: Biogeosciences*, 126, e2021JG006305. <https://doi.org/10.1029/2021JG006305>

Johnson, M. S., Matthews, E., Du, J., Genovese, V., & Bastviken, D. (2022). Methane emission from global lakes: New spatiotemporal data and observation driven modeling of methane dynamics indicates lower emissions. *Journal of Geophysical Research: Biogeosciences*, 127, e2022JG006793. <https://doi.org/10.1029/2022JG006793>

Jones, L. A., Kimball, J. S., Reichle, R. H., Madani, N., Glassy, J., Ardizzone, J. V., Colliander, A., Cleverly, J., Desai, A. R., Eamus, D., Euskirchen, E. S., Hutley, L., Macfarlane, C., & Scott, R. L. (2017). The SMAP level 4 carbon product for monitoring ecosystem land-atmosphere CO<sub>2</sub> exchange. *IEEE Transactions on Geoscience and Remote Sensing*, 55, 6517–6532.

Jung, M., Schwalm, C., Migavacca, M., Walther, S., Camps-Valls, G., Koitala, S., Anthoni, P., Besnard, S., Bodesheim, P., Carvalhais, N., Chevallier, F., Gans, F., Goll, D. S., Haverd, V., Köhler, P., Ichii, K., Jain, A. K., Liu, J., Lombardozzi, D., ... Reichstein, M. (2020). Scaling carbon fluxes from eddy covariance sites to globe: Synthesis and evaluation of the FLUXCOM approach. *Biogeosciences*, 17, 1343–1365.

Kim, Y., Kimball, J. S., Zhang, K., Didan, K., Velicongna, I., & McDonald, K. C. (2014). Attribution of divergent northern vegetation growth responses to lengthening non-frozen season optical-NIR and microwave remote sensing. *International Journal of Remote Sensing*, 35, 3700–3721.

Kim, Y., Kimball, J. S., Zhang, K., & McDonald, K. C. (2012). Satellite detection of increasing northern hemisphere non-frozen seasons from 1979 to 2008: Implications for regional vegetation growth. *Remote Sensing of Environment*, 121, 472–487.

Kimball, J. S., Jones, L. A., Glassy, J., & Reichle, R. (2016). SMAP L4 global daily 9 km carbon net ecosystem exchange, version 2. NASA National Snow and Ice Data Center Distributed Active Archive Center. <https://doi.org/10.5067/UBKO5ZUI715V>

Kimball, J. S., Jones, L. A., Zhang, K., Heinsch, F. A., McDonald, K. C., & Oechel, W. C. (2009). A satellite approach to estimate land-atmosphere CO<sub>2</sub> exchange for boreal and Arctic biomes using MODIS and AMSR-E. *IEEE Transactions on Geoscience and Remote Sensing*, 47, 569–587.

Kimball, J. S., Reichle, R., O'Neill, P., McDonald, K., & Njoku, E. (2012). SMAP Level 4 Carbon Data Product (L4\_C). Technical Document Prepared for the NASA SMAP Mission. [https://asf.alaska.edu/wp-content/uploads/2019/03/l4\\_c\\_initrel\\_v1\\_filt\\_10.pdf](https://asf.alaska.edu/wp-content/uploads/2019/03/l4_c_initrel_v1_filt_10.pdf)

Kirches, G., Brockmann, M. B., Peters, M., Bontemps, S., Lamarche, C., Schlerf, M., Santoro, M., & Defourny, P. (2014). CCI-LC product user guide. Esakia.

Kuhn, M. A., Varner, R. K., Bastviken, D., Crill, P., MacIntyre, S., Turetsky, M., Walter Anthony, K., McGuire, A. D., & Olefeldt, D. (2021). BAWLD-CH<sub>4</sub>: A comprehensive dataset of methane fluxes from boreal and arctic ecosystems. *Earth System Science Data*, 13, 5151–5189.

Laine, A. M., Mehtatalo, L., Tolvanen, A., Frolking, S., & Tuittila, E.-S. (2019). Impacts of drainage, restoration and warming on boreal wetland greenhouse gas fluxes. *Science of the Total Environment*, 647, 169–181.

Lasslop, G., Geichstein, M., Papale, D., Richardson, A. D., Arneth, A., Barr, A., Stoy, P., & Wohlfahrt, G. (2010). Separation of net ecosystem exchange into assimilation and respiration using a light response curve approach: Critical issues and global evaluation. *Global Change Biology*, 16, 187–208.

Lauvaux, T., Schuh, A. E., Bocquet, M., Wu, L., Richardson, S., Miles, N., & Davis, K. J. (2012). Network design for mesoscale inversions of CO<sub>2</sub> sources and sinks. *Tellus Series B: Chemical and Physical Meteorology*, 64, 17980. <https://doi.org/10.3402/tellusb.v6410.17980>

Le Quéré, C., Moriarty, R., Andrew, R. M., Canadell, J. G., Sitch, S., Korsbakken, J. I., Friedlingstein, P., Peters, G. P., Andres, R. J., Boden, T. A., Houghton, R. A., House, J. I., Keeling, R. F., Tans, P., Arneth, A., Bakker, D. C. E., Barbero, L., Bopp, L., Chang, J., et al. (2015). Global carbon budget 2015. *Earth System Science Data*, 7, 349–396.

Lehner, B., & Döll, P. (2004). Development and validation of a global database of lakes, reservoirs and wetlands. *Journal of Hydrology*, 296, 1–22.

Li, Z.-L., Mu, C.-C., Chen, X., Wang, X.-Y., Dong, W.-W., Jia, L., Mu, M., Streletskaya, I., Grebenets, V., Sokratov, S., Kizyakov, A., & Wu, X.-D. (2021). Changes in net ecosystem exchange of CO<sub>2</sub> in Arctic and their relationships with climate change during 2002–2017. *Advances in Climate Change Research*, 12, 475–481.

Lin, X., Rogers, B. M., Sweeney, C., Chevallier, F., Arshinov, M., Dlugokencky, E., Machida, T., Sasakawa, M., Tans, P., & Keppel-Aleks, G. (2020). Siberian and temperate ecosystems shape northern hemisphere atmospheric CO<sub>2</sub> seasonal amplification. *Proceedings of the National Academy of Sciences of the United States of America*, 117, 21079–21087. <https://doi.org/10.1073/pnas.1914135117>

Liu, Z., Kimball, J. S., Ballantyne, A. P., Parazoo, N. C., Wang, W. J., Bastos, A., Madani, N., Natali, S. M., Watts, J. D., Rogers, B. M., Ciais, P., Yu, K., Virkkala, A.-M., Chevallier, F., Peters, W., Patra, P. K., & Chandra, N. (2022). (In Revision) Respiratory loss during late-growing season determines the net carbon dioxide sink along the tree cover-permafrost gradient in northern high latitude regions. *Nature Communications*, 13, 5626. <https://doi.org/10.1038/s41467-022-33293-x>

Liu, Z., Kimball, J. S., Parazoo, N. C., Ballantyne, A. P., Wang, W. J., Madani, N., Pan, C. G., Watts, J. D., Reichle, R. H., Sonnentag, O., Marsh, P., Hurkuck, M., Helbig, M., Quinton, W. L., Zona, D., Ueyama, M., Kobayashi, H., & Euskirchen, E. S. (2020). Increased high-latitude photosynthetic carbon gain offset by respiration carbon loss during an anomalous warm winter to spring transition. *Global Change Biology*, 26, 682–696.

Loboda, T. V., Hoy, E. E., & Carroll, M. L. (2017). ABoVE: Study domain and standard reference grids. ORNL DAAC. <https://doi.org/10.3334/ORNLDAAAC/1367>

Lopez-Blanco, E., Exbrayat, J.-F., Lund, M., Christensen, T. R., Tamstorf, M. P., Dlevin, D., Hugelius, G., Bloom, A. A., & Williams, M. (2019). Evaluation of terrestrial pan-Arctic carbon cycling using a data-assimilation system. *Earth System Dynamics*, 10, 233–255.

Mastepanov, M., Sigsgaard, C., Dlugokencky, E. J., Houweling, S., Strom, L., Tamstorf, M. P., & Christensen, T. R. (2008). Large tundra methane burst during onset of freezing. *Nature*, 456, 628–630.

McGuire, A. D., Christensen, T. R., Hayes, D. J., Heroult, A., Euskirchen, E., Yi, Y., Kimball, J. S., Koven, C., Lafleur, P., Miller, P. A., Oechel, W., Peylin, P., & Williams, M. (2012). An assessment of the carbon balance of arctic tundra: Comparisons among observations, process models, and atmospheric inversions. *Biogeosciences*, 9, 3185–3204.

Mekonnen, Z. A., Riley, W. J., Berner, L. T., Bouskill, N. J., Torn, M. S., Iwahana, G., Breen, A. L., Myers-Smith, I. H., Criado, M. G., & Liu, Y. (2021). Arctic tundra shrubification: A review of mechanisms and impacts on ecosystem carbon balance. *Environmental Research Letters*, 16, 053001.

Melton, J., Wania, R., Hodson, E., Poulter, B., Ringeval, B., Spahni, R., Bohn, T., Beerling, D., Chen, G., Eliseev, A., Denisov, S., Hopcroft, P., Lettenmaier, D., Riley, W., Singarayer, J., Subin, Z. M., Tian, H., Zürcher, S., Brovkin, V., ... Kaplan, J. O. (2013). Present state of global wetland extent and wetland methane modelling: Conclusions from a model inter-comparison project (WETCHIMP). *Biogeosciences*, 10, 753–788.

Miner, K. R., Turetsky, M. R., Malina, E., Bartsch, A., Tamminen, J., McGuire, A. D., Fix, A., Sweeney, C., Elder, C. D., & Miller, C. E. (2022). Permafrost carbon emissions in a changing Arctic. *Nature Reviews Earth & Environment*, 3, 55–67.

Myreni, R., Knyazikhin, Y., & Park, T. (2015). MCD15A3H MODIS/Terra + aqua leaf area index/FPAR 4-day L4 global 500m SIN grid V006. NASA EOSDIS Land Processes DAAC. <https://doi.org/10.5067/MODIS/MCD15A3H.006>

Natali, S. M., Holdren, J. P., Rogers, B. M., & MacDonald, E. (2021). Permafrost carbon feedbacks threaten global climate goals. *Proceedings of the National Academy of Sciences of the United States of America*, 118(21), e2100163118. <https://doi.org/10.1073/pnas.2100163118>

Natali, S. M., Watts, J. D., Rogers, B. M., Potter, S., Ludwig, S. M., Selbmann, A.-K., Sullivan, P. F., Abbott, B. W., Arndt, K. A., Birch, L., Bjorkman, M. P., Anthony Bloom, A., Celis, G., Christensen, T. R., Christiansen, C. T., Commane, R., Cooper, E. J., Crill, P., Czimczik, C., ... Zona, D. (2019). Large loss of CO<sub>2</sub> in winter observed across the northern permafrost region. *Nature Climate Change*, 9, 852–857.

Olefeldt, D., Euskirchen, E. S., Harden, J., Kane, E., David McGuire, A., Waldrop, M. P., & Turetsky, M. R. (2017). A decade of boreal rich fen greenhouse gas fluxes in response to natural and experimental water table variability. *Global Change Biology*, 23, 2428–2440.

Pallandt, M. M. T. A., Kumar, J., Mauritz, M., Schuur, E. A. G., Virkkala, A.-M., Celis, G., Hoffman, F. M., & Gockede, M. (2022). Representativeness assessment of the pan-Arctic eddy covariance site network and optimized future enhancements. *Biogeosciences*, 19, 559–583.

Pan, N., Feng, X., Fu, B., Wang, S., Ji, F., & Pan, S. (2018). Increasing global vegetation browning hidden in overall vegetation greening: Insights from time-varying trends. *Remote Sensing of Environment*, 214, 59–72.

Pan, Y., Birdsey, R. A., Fang, J., Houghton, R., Kauppi, P. E., Kurz, W. A., Phillips, O. L., Shvidenko, A., Lewis, S. L., Canadell, J. G., Ciais, P., Jackson, R. B., Pacala, S. W., McGuire, A. D., Piao, S., Rautiainen, A., Sitch, S., & Hayes, D. (2011). A large and persistent carbon sink in the world's forests. *Science*, 333, 988–993.

Parazoo, N. C., Commane, R., Wofsy, S. C., Koven, C. D., Sweeney, C., Lawrence, D. M., Lindaas, J., Chang, R. Y.-W., & Miller, C. E. (2016). Detecting regional patterns of changing CO<sub>2</sub> flux in Alaska. *Proceedings of the National Academy of Sciences of the United States of America*, 113, 7733–7738.

Peltola, O., Vesala, T., Gao, Y., Räty, O., Alekseychik, M. A., Chojnicki, B., Desai, A. R., Dolman, A. J., Euskirchen, E. S., Friborg, T., Gockede, M., Helbig, M., Humphreys, E., Jackson, R. B., Jocher, G., Joos, F., Klatt, J., Knox, S. H., Kowalska, N., ... Aalto, T. (2019). Monthly gridded data product of northern wetland methane emissions based on upscaling eddy covariance observations. *Earth System Science Data*, 11, 1263–1289.

Peng, C., Ma, Z., Lei, X., Zhu, Q., Chen, H., Wang, W., Liu, S., Li, W., Fang, X., & Zhou, X. (2011). A drought-induced pervasive increase in tree mortality across Canada's boreal forests. *Nature Climate Change*, 1, 467–471.

Phillips, C. A., Rogers, B. M., Elder, M., Cooperdock, S., Moubarak, M., Randerson, J. T., & Frumhoff, P. C. (2022). Escalating carbon emissions from north American boreal forest wildfires and the climate mitigation potential of fire management. *Science Advances*, 8, eabl7161. <https://doi.org/10.1126/sciadv.abl7161>

Phoenix, G. K., & Bjerke, J. W. (2016). Arctic browning: Extreme events and trends reversing arctic greening. *Global Change Biology*, 22, 2960–2962.

R Core Team. (2019). *R: A language and environment for statistical computing*. R Foundation for Statistical Computing. <http://www.R-project.org>

Rantanen, M., Karpechko, A. Y., Lipponen, A., Nordling, K., Hyvarinen, O., Ruosteenoja, K., Vihma, T., & Laaksonen, A. (2022). The Arctic has warmed nearly four times faster than the globe since 1979. *Nature Communications Earth & Environment*, 3, 168.

Raz-Yaseef, N., Torn, M. S., Wu, Y., Billesbach, D. P., Liljedahl, A. K., Kneafsey, T. J., Romanovsky, V. E., Cook, D. R., & Wullschleger, S. D. (2017). Large CO<sub>2</sub> and CH<sub>4</sub> emissions from polygonal tundra during spring thaw in northern Alaska. *Geophysical Research Letters*, 44, 504–513.

Reichle, R. H., Koster, R. D., De Lannoy, G. J. M., Forman, B. A., Liu, Q., Mahanama, S. P. P., & Toure, A. (2011). Assessment and enhancement of MERRA land surface hydrology estimates. *Journal of Climate*, 24, 6322–6338.

Reichstein, M., Stoy, P. C., Desai, A. R., Lasslop, G., & Richardson, A. R. (2012). Partitioning of net fluxes. In M. Aubinet, et al. (Eds.), *Eddy covariance: A practical guide to measurement and data analysis* (pp. 263–298). Springer Atmospheric Sciences. <https://doi.org/10.1007/978-94-007-2351-9>

Ribeiro-Kumara, C., Koster, E., Aaltonen, H., & Koster, K. (2020). How do forest fires affect soil greenhouse gas emissions in upland boreal forests? A review. *Environmental Research*, 184, 109328. <https://doi.org/10.1016/j.envres.2020.109328>

Rienecker, M. M., Suarez, M. J., Gelaro, R., Todling, R., Bacmeister, J., Liu, E., Bosilovich, M. G., Schubert, S. D., Takacs, L., Kim, G. K., Bloom, S., Chen, J., Collins, D., Conaty, A., da Silva, A., Gu, W., Joiner, J., Koster, R. D., Lucchesi, R., ... Woollen, J. (2011). MERRA: NASA's modern-era retrospective analysis for research and applications. *Journal of Climate*, 24, 3624–3648.

Rinne, J., Tuovinen, J.-P., Klemetsson, L., Aurela, M., Holst, J., Lohila, A., Weslien, P., Vestin, P., Lakomiec, P., Peichl, M., Tuittila, E.-S., Heiskanen, L., Laurila, T., Li, X., Alekseychik, A., Mammarella, I., Strom, L., Crill, P., & Nilsson, M. B. (2020). Effect of the 2018 European drought on methane and carbon dioxide exchange of northern mire ecosystems. *Philosophical Transactions of the Royal Society B: Biological Sciences*, 375, 20190517. <https://doi.org/10.1098/rstb.2019.0517>

Rogers, B. M., Solvik, K., Hogg, E. H., Ju, J., Masek, J. G., Michaelian, M., Berner, L. T., & Goetz, S. J. (2018). Detecting early warning signals of tree mortality in boreal North America using multiscale satellite data. *Global Change Biology*, 24, 2284–2304. <https://doi.org/10.1111/gcb.14107>

Running, S. W., Nemani, R. R., Heinsch, F. A., Zhao, M., Reeves, M., & Hashimoto, H. (2004). A continuous satellite-derived measure of global terrestrial primary production. *BioScience*, 54(6), 547–560.

Sato, H., Kobayashi, H., Iwahana, G., & Ohta, T. (2016). Endurance of larch forest ecosystems in eastern Siberia under warming trends. *Ecology and Evolution*, 6, 5690–5704.

Schädel, C., Bader, M. K. F., Schuur, E. A. G., Biasi, C., Brancho, R., Čapek, P., De Baets, S., Diáková, K., Ernakovich, J., Estop-Aragones, C., Graham, D. E., Hartley, I. P., Iversen, C. M., Kane, E., Knoblauch, C., Lupascu, M., Martikainen, P. J., Natali, S. M., Norby, R. J., ... Wickland, K. P. (2016). Potential carbon emissions dominated by carbon dioxide from thawed soils. *Nature Climate Change*, 6, 950–953.

Schiferl, L. D., Watts, J. D., Larson, E. J. L., Arndt, K. A., Biraud, S. C., Euskirchen, E. S., Goodrich, J. P., Henderson, J. M., Kalhori, A., McKain, K., Mountain, M. E., Munger, J. W., Oechel, W. C., Sweeney, C., Yi, Y., Zona, D., & Commane, R. (2022). Using atmospheric observations to quantify annual biogenic carbon dioxide fluxes on the

Alaska North Slope. *Biogeosciences*, 19, 5953–5972. <https://doi.org/10.5194/bg-19-5953-2022>

Schimel, D., Pavlick, R., Fisher, J. B., Asner, G. P., Saatchi, S., Townsend, P., Miller, C., Frankenberg, C., Hibbard, K., & Cox, P. (2015). Observing terrestrial ecosystems and the carbon cycle from space. *Global Change Biology*, 21, 1762–1776.

Schuh, A. E., Lauvaux, T., West, T. O., Denning, A. S., Davis, K. J., Miles, N., Richardson, S., Uliasz, M., Lokupitiya, E., Cooley, D., Andrews, A., & Ogle, S. (2013). Evaluating atmospheric CO<sub>2</sub> inversions at multiple scales over a highly inventoried agricultural landscape. *Global Change Biology*, 19, 1424–1439.

Schulze, E.-D. (2006). Biological control of the terrestrial carbon sink. *Biogeosciences*, 3, 147–166.

Schulze, E.-D., Loyd, J., Kelliher, F. M., Wirth, C., Rebmann, C., Luhker, B., Mund, M., Knohl, A., Milyukova, I. M., Schulze, W., Ziegler, W., Varlagin, A. B., Sogachev, A. F., Valentina, R., Dore, S., Grigoriev, S., Kolle, O., Panfyorov, I., Tchekabkova, N., & Vygodskaya, N. N. (1999). Productivity of forests in the Eurosiberian boreal region and their potential to act as a carbon sink—A synthesis. *Global Change Biology*, 5, 703–722.

Schuur, E. A. G., Abbott, B. W., Commane, R., Ernakovich, J., Euskirchen, E., Hugelius, G., Grosse, G., Jones, M., Koven, C., Leshyk, V., Lawrence, D., Loranty, M. M., Mauritz, M., Olefeldt, D., Natali, S., Rodenhizer, H., Salmon, V., Schädel, C., Strauss, J., ... Turetsky, M. (2022). Permafrost and climate change: Carbon cycle feedbacks from the warming arctic. *Annual Review of Environment and Resources*, 47, 343–371.

Schuur, E. A. G., & Mack, M. C. (2018). Ecological response to permafrost thaw and consequences for local and global ecosystem services. *Annual Review of Ecology, Evolution, and Systematics*, 49, 279–301.

Schuur, E. A. G., McGuire, A. D., Schadel, C., Grosse, G., Harden, J. W., Hayes, D. J., Hugelius, G., Koven, C. D., Kuhry, P., Lawrence, D. M., Natali, S. M., Olefeldt, D., Romanovsky, V. E., Schaefer, K., Turetsky, M. R., Treat, C. C., & Vonk, J. E. (2015). Climate change and the permafrost carbon feedback. *Nature*, 520, 171–179.

Shvetsov, E. G., Kukavskaya, E. A., Shestakov, T. A., Laflamme, J., & Rogers, B. M. (2021). Increasing fire and logging disturbances in Siberian boreal forests: A case study of the Angara region. *Environmental Research Letters*, 16, 115007.

Stanley, E. H., Loken, L. C., Casson, N. J., Oliver, S. K., Sponseller, R. A., Wallin, M. B., Zhang, L., & Rocher-Ros, G. (2022). GRiMeDB: The global river database of methane concentrations and fluxes. *Earth System Science Data Discussions*. <https://doi.org/10.5194/essd-2022-346>

Stocker, B. D., Spahni, R., & Joos, F. (2014). DYTOP: A cost-efficient TOPMODEL implementation to simulate sub-grid spatio-temporal dynamics of global wetlands and peatlands. *Geoscientific Model Development*, 7, 3089–3110.

Stoy, P. C., Katul, G. G., Siqueira, M. B. S., Juang, J.-Y., Novick, K. A., Uebelherr, J. M., & Oren, R. (2006). An evaluation of models for partitioning eddy covariance-measured net ecosystem exchange into photosynthesis and respiration. *Agricultural and Forest Meteorology*, 141, 2–18.

Strom, L., & Christensen, T. R. (2007). Belowground carbon turnover and greenhouse gas exchanges in a sub-arctic wetland. *Soil Biology and Biochemistry*, 39, 1689–1698.

Sulla-Menashe, D., Woodcock, C. E., & Friedl, M. A. (2018). Canadian boreal forest greening and browning trends: An analysis of biogeographic patterns and the relative roles of disturbance versus climate drivers. *Environmental Research Letters*, 13, 014007. <https://doi.org/10.1088/1748-9326/aa9b88>

Sun, Q., Burrell, A., Barrett, K., Kukavskaya, E., Buryak, L., Kaduk, J., & Baxter, R. (2021). Climate variability may delay post-fire recovery of boreal forest in southern Siberia, Russia. *Remote Sensing*, 13, 2247. <https://doi.org/10.3390/rs13122247>

Sweeney, C., Chatterjee, A., Wolter, S., McKain, K., Bogue, R., Newberger, T., Hu, L., Ott, L., Poulter, B., Schiferl, L. D., Weir, B., Zhang, Z., & Miller, C. E. (2020). Atmospheric carbon cycle dynamics over the ABoVE domain: An integrated analysis using aircraft observations (Arctic-CAP) and model simulations (GEOS). *Atmospheric Chemistry and Physics*. <https://doi.org/10.5194/acp-2020-609>

Tagesson, T., Schurges, G., Horion, S., Ciais, P., Tian, F., Brandt, M., Ahlstrom, A., Wigéron, J.-P., Ardo, J., Olin, S., Fan, L., Wu, Z., & Fensholt, R. (2020). Recent divergence in the contributions of tropical and boreal forests to the terrestrial carbon sink. *Nature Ecology and Evolution*, 4, 202–209.

Tan, Z., Zhuang, Q., Henz, D. K., Frankenberg, C., Dlugokencky, E., Sweeney, C., Turner, A. J., Sasakawa, M., & Machida, T. (2016). Inverse modeling of pan-Arctic methane emissions at high spatial resolution: What can we learn from assimilating satellite retrievals and using different process-based wetland and lake biogeochemical models? *Atmospheric Chemistry and Physics*, 16, 12649–12666.

Thompson, R. L., Sasakawa, M., Machida, T., Aalto, T., Worthy, D., Lavric, J. V., Lund Myhre, C., & Stohl, A. (2017). Methane fluxes in the high northern latitudes for 2005–2013 estimated using a Bayesian atmospheric inversion. *Atmospheric Chemistry and Physics*, 17, 3553–3572.

Turetsky, M. R., Abbott, B. W., Jones, M. C., Anthony, K. W., Olefeldt, D., Schuur, E. A. G., Koven, C., McGure, A. D., Grosse, G., Kuhry, P., Hugelius, G., Lawrence, D. M., Gibson, C., & Sannel, A. B. K. (2019). Permafrost collapse is accelerating carbon release. *Nature*, 569, 32–34.

Turetsky, M. R., Kotowska, A., Bubier, J., Dise, N. B., Crill, P., Hornbrook, E. R., Minkkinen, K., Moore, T. R., Myers-Smith, I. H., Nykänen, H., & Olefeldt, D. (2014). A synthesis of methane emissions from 71 northern, temperate, and subtropical wetlands. *Global Change Biology*, 7, 2183–2197.

Ueyama, M., Iwata, H., & Harazono, Y. (2014). Autumn warming reduces the CO<sub>2</sub> sink of a black spruce forest in interior Alaska based on a nine-year eddy covariance measurement. *Global Change Biology*, 20, 1161–1173.

Ueyama, M., Kazuhito, I., Iwata, H., Euskirchen, E. S., Zona, D., Rocha, A. V., Harazono, Y., Iwama, C., Nakai, T., & Oechel, W. C. (2013). Upscaling terrestrial carbon dioxide fluxes in Alaska with satellite remote sensing and support vector regression. *Journal of Geophysical Research: Biogeosciences*, 118, 1266–1281. <https://doi.org/10.1002/jgr.20095>

van Wees, D., van der Werf, G. R., Randerson, J. T., Rogers, R. M., Chen, Y., Veraverbeke, S., Giglio, L., & Morton, D. C. (2022). Global biomass burning fuel consumption and emissions at 500 m spatial resolution based on the Global Fire Emissions Database (GFED). *Geoscientific Model Development*, 15, 8411–8437. <https://doi.org/10.5194/gmd-15-8411-2022>

Veraverbeke, S., Delcourt, C. J. F., Kukavskaya, E., Mack, M., Walker, X., Hessilt, T., Rogers, B., & Scholten, R. C. (2021). Direct and longer-term carbon emissions from arctic-boreal fires: A short review of recent advances. *Current Opinion in Environmental Science & Health*, 23, 100277. <https://doi.org/10.1016/j.coesh.2021.100277>

Virkkala, A.-M., Aalto, J., Rogers, B. M., Tagesson, T., Treat, C. C., Natali, S. M., Watts, J. D., Potter, S., Lehtonen, A., Mauritz, M., Schuur, E. A. G., Kochendorfer, J., Zona, D., Oechel, W., Kobayashi, H., Humphreys, E., Goeckede, M., Iwata, H., Lafleur, P. M., ... Luoto, M. (2021). Statistical upscaling of ecosystem CO<sub>2</sub> fluxes across the terrestrial tundra and boreal domain: Regional patterns and uncertainties. *Global Change Biology*, 27, 4040–4059.

Virkkala, A.-M., Natali, S. M., Rogers, B. M., Watts, J. D., Savage, K., Connon, S. J., Mauritz, M., Schuur, E. A. G., Peter, D., Minions, C., Nojeim, J., Commane, R., Emmerton, C. A., Goeckede, M., Helbig, M., Holl, D., Iwata, H., Kobayashi, K. P., Lopez-Blanco, E., ... Zyryanov, V. I. (2022). The ABCflux database: Arctic-boreal CO<sub>2</sub> flux observations and ancillary information aggregated to monthly

time steps across terrestrial ecosystems. *Earth System Science Data*, 14, 179–208.

Vitt, D. H. (2006). Functional characteristics and indicators of boreal peatlands. In R. K. Wieder & D. H. Vitt (Eds.), *Boreal peatland ecosystems: ecological studies (analysis and synthesis)* (Vol. 188). Springer.

Walker, D. A., Raynolds, M. K., Daniels, F. J. A., Einarsson, E., Elvebakk, A., Gould, W. A., Katenin, A. E., Kholod, S. S., Markon, C. J., Melnikov, E. S., Moskaleko, N. G., Talbot, S. S., & Yurtsev, B. A. (2005). The circumpolar Arctic vegetation map. *Journal of Vegetation Science*, 16, 267–282.

Walker, W. S., Gorelik, S. R., Cook-Patton, S. C., Baccini, A., Farina, M. K., Solvik, K. K., Ellis, P. W., Sanderman, J., Houghton, R. A., Leavitt, S. M., Schwalm, C. R., & Griscom, B. W. (2022). The global potential for increased storage of carbon on land. *Proceedings of the National Academy of Sciences of the United States of America*, 119, e2111312119.

Walker, X. J., Baltzer, J. L., Cumming, S. G., Day, N. J., Ebert, C., Goetz, S., Johnstone, J. F., Potter, S., Rogers, B. M., Schuur, E. A. G., Turetsky, M. R., & Mack, M. C. (2019). Increasing wildfires threaten historic carbon sink of boreal forest soils. *Nature*, 572, 520–523.

Wang, J., Sulla-Menashe, D., Woodcock, C. E., Sonnentag, O., Keeling, R. F., & Friedl, M. A. (2020). Extensive land cover change across Arctic-boreal northwestern North America from disturbance and climate forcing. *Global Change Biology*, 26, 807–822.

Wang, Y., Yuan, F., Yuan, F., Gu, B., Hahn, M. S., Torn, M. S., Ricciuto, D. M., Kumar, J., Zona, L. H. D., Lipson, D. A., Wagner, R., Oechel, W. C., Wullschleger, S. D., Thornton, P. E., & Xu, X. (2019). Mechanistic modeling of microtopographic impacts on  $\text{CO}_2$  and  $\text{CH}_4$  fluxes in an Alaskan tundra ecosystem using the CLM-microbe model. *JAMES*, 11, 4288–4304.

Ware, J., Kort, E. A., Duren, R., Mueller, K. L., Verhulst, K., & Yadav, V. (2019). Detecting urban emissions changes and events with a near-real-time-capable inversion system. *JGR Atmospheres*, 124, 5117–5130.

Watts, J. D., Kimball, J. S., Bartsch, A., & McDonald, K. C. (2014). Surface water inundation in the boreal-Arctic: Potential impacts on regional methane emissions. *Environmental Research Letters*, 9, 1–13.

Watts, J. D., Kimball, J. S., Parmentier, F.-J. W., Sachs, T., Rinne, J., Zona, D., Oechel, W., Tagesson, T., Jackowicz-Korczyński, M., & Aurela, M. (2014). A satellite data driven biophysical modeling approach for estimating northern peatland and tundra  $\text{CO}_2$  and  $\text{CH}_4$  fluxes. *Biogeosciences*, 11, 1961–1980.

Watts, J. D., Natali, S. M., Minions, C., Risk, D., Arndt, K., Zona, D., Euskirchen, E. S., Rocha, A. V., Sonnentag, O., Helbig, M., Kalhor, A., Oechel, W., Ikawa, H., Ueyama, M., Suzuki, R., Kobayashi, H., Celis, G., Schuur, E. A. G., Humphreys, E., ... Edgar, C. (2021). Soil respiration strongly offsets carbon uptake in Alaska and Northwest Canada. *Environmental Research Letters*, 16, 084051.

Webb, J. R., Santos, I. R., Maher, D. T., & Finlay, K. (2019). The importance of aquatic carbon fluxes in net ecosystem carbon budgets: A catchment-scale review. *Ecosystems*, 22, 508–527.

Welp, L. R., Patra, P. K., Rodenbeck, C., Nemani, R., Bi, J., Piper, S. C., & Keeling, R. F. (2016). Increasing summer net  $\text{CO}_2$  uptake in high northern ecosystems inferred from atmospheric inversions and comparisons to remote-sensing NDVI. *Atmospheric Chemistry and Physics*, 16, 9047–9066.

White, A., Cannell, M. G. R., & Friend, A. D. (2001). The high-latitude terrestrial carbon sink: A model analysis. *Global Change Biology*, 6, 227–245.

Whitman, E., Parisien, M. A., Thompson, D. K., & Flannigan, M. D. (2019). Short-interval wildfire and drought overwhelm boreal forest resilience. *Scientific Reports*, 9, 18796. <https://doi.org/10.1038/s41598-019-55036-7>

Wrona, F. J., Johansson, M., Culp, J. M., Jenkins, A., Mard, J., Myers-Smith, I. H., Prowse, T. D., Vincent, W. F., & Wookey, P. A. (2016). Transitions in Arctic ecosystems: Ecological implications of a changing hydrological regime. *Journal of Geophysical Research: Biogeosciences*, 121, 650–674.

Xu, J., Morris, P. J., Liu, J., & Holden, J. (2018). PEATMAP: Refining estimates of global peatland distribution based on a meta-analysis. *Catena*, 160, 134–140.

Yi, X., Kimball, J. S., Jones, L. A., Reichle, R. H., & McDonald, K. C. (2011). Evaluation of MERRA land surface estimation in preparation for the soil moisture active passive Mission. *Journal of Climate*, 24, 3797–3816.

Zhang, Z., Zimmermann, N. E., Stenke, A., & Poulter, B. (2017). Emerging role of wetland methane emissions in driving 21st century climate change. *Proceedings of the National Academy of Sciences of the United States of America*, 114, 9647–9652.

Zhao, B., Zhuang, Q., Shurpali, N., Koster, K., Berninger, F., & Pumpanen, J. (2021). North American boreal forests are a large carbon source due to wildfires in 1986 to 2016. *Scientific Reports*, 11, 7723.

Zona, D., Gioli, B., Commane, R., Lindaas, J., Wofsy, S. C., Miller, C. E., Dinardo, S. J., Dengel, S., Sweeney, C., Karion, A., Chang, R. Y.-W., Henderson, J. M., Murphy, P. C., Goodrich, J. P., Moreaux, V., Liljedahl, A., Watts, J. D., Kimball, J. S., Lipson, D. A., & Oechel, W. C. (2016). Cold season emissions dominate the Arctic tundra methane budget. *Proceedings of the National Academy of Sciences of the United States of America*, 113, 40–45.

Zona, D., Lafleur, P. M., Hufkens, K., Bailey, B., Gioli, B., Burba, G., Goodrich, J. P., Liljedahl, A. K., Euskirchen, E. S., Watts, J. D., Farina, M., Kimball, J. S., Heimann, M., Göckede, M., Pallandt, M., Christensen, T. R., Mastepanov, M., López-Blanco, E., Jackowicz-Korczynski, M., ... Oechel, W. C. (2022). Earlier snowmelt may lead to late season declines in plant productivity and carbon sequestration in Arctic tundra ecosystems. *Scientific Reports*, 12, 1–10.

## SUPPORTING INFORMATION

Additional supporting information can be found online in the Supporting Information section at the end of this article.

**How to cite this article:** Watts, J. D., Farina, M., Kimball, J. S., Schiferl, L. D., Liu, Z., Arndt, K. A., Zona, D., Ballantyne, A., Euskirchen, E. S., Parmentier, F.-J., Helbig, M., Sonnentag, O., Tagesson, T., Rinne, J., Ikawa, H., Ueyama, M., Kobayashi, H., Sachs, T., Nadeau, D. F. ... Oechel, W. C. (2023). Carbon uptake in Eurasian boreal forests dominates the high-latitude net ecosystem carbon budget. *Global Change Biology*, 29, 1870–1889. <https://doi.org/10.1111/gcb.16553>